



**University of  
Zurich**<sup>UZH</sup>

# Age Determination of a Mire in the Wind River Range Area, Wyoming.

GEO 511 Master's Thesis

**Author**

Mike Dumitrescu

13-739-321

**Supervised by**

Prof. Dr. Markus Egli

**Faculty representative**

Prof. Dr. Markus Egli

01.09.2019

Department of Geography, University of Zurich



University of  
Zurich<sup>UZH</sup>

# Age Determination of a Mire in the Wind River Range Area, Wyoming.

31.08.2019

Thesis supervisor:  
Prof. Dr. Markus Egli  
Department of Geography  
UZH - University of Zurich



Last name: Dumitrescu  
First name: Mike Kevin  
Matriculation no. 13-739-321  
E-Mail: [mike.dumitrescu@uzh.ch](mailto:mike.dumitrescu@uzh.ch)  
Telephone: +41 76 587 24 48  
Adress: Irchelstrasse 75; 8400 Winterthur

# Table of Contents

Abstract	3
1.1 Introduction	4
1.2 Research Question	5
1.3 Research Area	6
1.4 Mire and soil Samples	7
1.4.1 Sampling strategy and sample preparation	7
1.4.2 Sample preparation	8
2. Methods	9
2.1 Grain Size	9
2.2 pH	9
2.3 Atomic Absorption Spectrometry (AAS)	10
2.3.2 Oxalate extraction	10
2.3.3 Dithionite extraction	10
2.4 XRD	11
2.4.1 Clay minerals and their response to the various treatments	13
2.5 X-Ray Fluorescence (XRF)	14
2.6 Diffuse Reflectance Infrared Fourier Transformation (Drift)	14
2.7 Loss of Ignition (LOI)	15
2.8 Total Carbon Content - Combusting Method	15
2.9 C14	15
3. Results	16
3.1 Soils	18
3.1.2 Dithionite Extraction of the soils	21
3.1.3 Clay Minerals of the soils	21
3.2 Mire Cores	24
3.2.1 pH, LOI & Bulk density	24
3.2.2 C14 Dating of the mire deposits	28
3.2.3 Elemental contents of the mire	31
4. Discussion	39
5. Conclusion	46
6. Acknowledgments	47
7. References	48

# Abstract

High mountains having a cold climate such as the Wind River Range area belong to the geomorphologically most active areas of the world with a variety of landscape forming processes.

The Wind River Range has been strongly affected by different glaciations and has several type localities for glacier surges (such as Pinedale, Bull Lake). How cold and warm phases influenced soil formation and erosion is poorly understood for this region. We hypothesised that signals of progressing and regression soil formation phases can be detected in mires near the Dickinson Park not only for the Holocene but also for older periods. In addition, the Holocene was alternately characterized by cold and warm phases, but it is not yet very clear how these phases changed the environment. With the help of mires, landscape processes can be reconstructed and an insight can be gained into the current situation at that time. Related research questions were: how does the age depth trend look like in the mire? how do the sediment rates change over time? how can these sedimentation rates be related to the climate? Mires are considered as geologic archives. Using radiocarbon dating of the organic matter remains in the mires and the dating of the surrounding moraines ( $^{10}\text{Be}$ ), a temporal framework of the environmental processes over time was achieved. The environmental processes of the last 10ka were reconstructed with the help of chemical investigations of the mires and the surrounding soils profiles. We detected that the mire reaches different maximum ages at different places (about 3 – 11 ka). In contrast to the expectations, no older ages could be measured. The mire therefore only covers the Holocene and signals of the Pleistocene seem entirely absent.

The depth trends were in all cases not constant and showed pronounced phases with higher and lower rates (0.7-0.1 cm/yr). As a consequence, the derived sedimentation rates exhibited a pronounced spatio-temporal variability. Some mire profiles clearly showed, that more weathered material (soils) was deposited during the last 5 kyr. The different profiles within the mire also did not always react similarly to climate fluctuations during the Holocene. Some profiles only react with a delay after a cold phase, others do not react at all regarding the sedimentation rate change.

However, the sedimentation rate usually increased after a cold period. So we have a sedimentation rate increase after 2.6 ka, 4.2ka, 6ka and 8ka. The chemical signatures in the mires demonstrated that deposited material is coming from local sources and is characterized by granitic properties. LOI and pH values show a high local variability.

## 1.1 Introduction

The change from the last glacier maximum to today's interglacial gives important information and a better understanding of how the Earth's climate system can abruptly and rapidly change from one status to another (Yu & Eichler, 2019). Since the last glacier maximum about 19000-23000 years ago the climate has changed radically in short time and the environment reacted accordingly.

The Pleistocene is characterized by strong climatic fluctuations. Cold and warm periods alternated. During the climate warming in the Holocene, the landscape changed, the glaciers retreated and the physical processes changed. Especially in areas strongly affected by glaciation, climate change plays an important role. Due to temperature changes of 2°C, glaciers in some parts of the world are decreasing to 5-10% of the glacier level (Leonard, et al., 2014). This retreat and its consequences are very important to study in detail the glaciers that have a major impact on their environment. Mountain ranges (like the Wind River Range; see below) are geomorphologically very active regions. Surface erosion by mass movements, snow avalanches, mudflows or solifluction are some processes among many taking place in such areas. For various reasons, mountain ecosystems react particularly strongly to changing environmental conditions. Global warming, atmospheric nutrient input, and acid deposition play an important role (Mavris, et al., 2015). Ecosystems in turn have a major influence on soil formation processes (Yoo, et al.: 2007).

This raises the question of how soils and landscape co-evolve in high alpine regions and how they are related to climate change. The existing knowledge in this research is still incomplete and fragmented. With the help of mires, the changes of the climate in the past can be reconstructed. In the structure of mires and their properties signals of the past climate can be derived.

***“Mires (i.e. bogs, transition bogs and fens) are assumed to be especially vulnerable to climate change because they depend on specific, namely cool and humid, climatic conditions”(Essl, et. al.,2011).***

Mires are important natural archives when it comes to reconstructing climate change, environmental conditions and ecosystem change (Lamentowicz, et al., 2015). Already at the end of the 19th century the first peat stratigraphy of mires in Scandinavia was examined in detail (Chambers, et al., 2012). However, a few years passed before one had an understanding of how mires grow. Only then they could be used more accurately as climate archives (Chambers, et al., 2012). The work of Aaby (1976) in which he reported sub- Milanković -scale climate changes of the Late Holocene with the help of peat humification and rhizopoda (testate amoebae) or the work of Barber (1981), the mires were examined

more closely and these works are the cornerstones for a better understanding of mires and climate change. But Zoller (1966) and Burga (1979) also conducted intensive research on this topic, particularly in the Alps.

Since then, the research methods have evolved considerably and there are various research approaches dealing with mires and climate change. The current state-of-art methods for using proxy climate indicators of mires include biomarkers in peat, stable isotopes, inorganic chemistry, plant macrofossils, peat humification and others. (Langdon, et al., 2012). But these are by no means all the methods that can be used today for mires. An extensive list of different methods can be found in Chamber's work (2012).

But not all of these methods are applicable to all mires; so the methods have to be specifically selected for each mire (Langdon, et al., 2012). The methods for determining geochemical properties of mires open doors to draw conclusions about the past climate and related geomorphic processes. For example, element concentrations can be indicators of strong erosional events, dust input etc. (Chambers, et al., 2012, Boxleitner, et al., 2017)

## 1.2 Research Question

The main goal of this master thesis was to obtain more information about the past climate history by using a mire as environmental archive. The aim was to investigate how the mire and related deposits within the mire correlate to specific climate periods and how the mire developed in connection with its environment. In addition, the surrounding soils were investigated to decipher how their evolution and chemical signatures relate to chemical fingerprints of the mire. This should help in detecting progressive (phases with no disturbances) and regressive (strong erosional periods) soil development phases. In addition, the age of the mire had to be determined in order to chronologically determine the development of the mire.

Within this master thesis I would like to answer several questions. The first research question is, how old is the mire and what is the age trend within the mire (age – depth relationship). Do different profiles from the same mire differ in the age depth trend or are they all similar? The next question is: what is the sedimentation rate or mire upbuilding of the past and, therefore, how much material was deposited in the mire and can we correlate these sedimentation rates to elements such as Si and Al? Furthermore, how strong is the degree of weathering of the sedimented material and how does it change over time? Where does the material deposited in the mire come from? I hypothesize that the material in the mire must have ages of more than 50000 years. This hypothesis is based on the geomorphic settings, i.e. moraine ages, of the surroundings (see below). The depth age trend for the different mire profiles should be similar. In addition, I hypothesize that the sedimentation rate has changed over time and been determined by the prevailing climatic influences.

## 1.3 Research Area

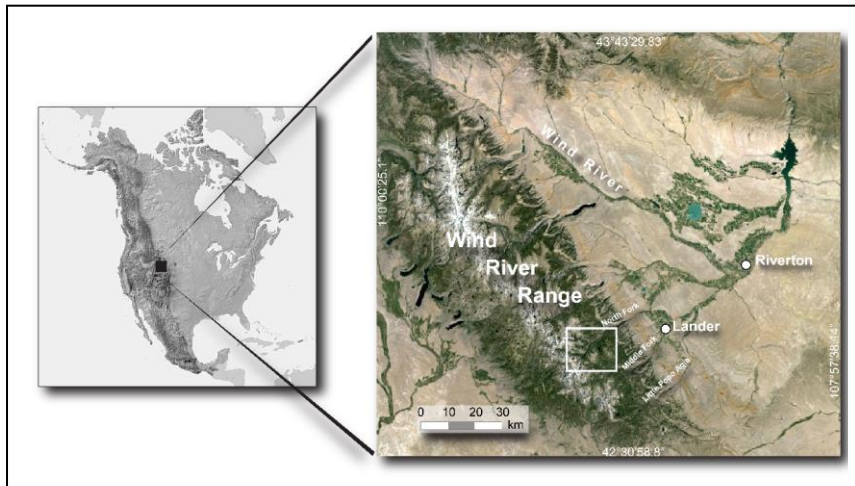


*Figure 1: The Research Area are located in the Wind River Range Area, which is a foothill of the Rocky Mountains, USA.*

The study area is in the Wind River District of Shoshone National Forest in Fremont Country, which is a mountain range of the Rocky Mountains located of west-central Wyoming, USA (Heidel, 2013). The Dickinson Park is on the east slope of the

Wind River Range and the next city is Lander, which is around 24-32 air kilometer away. The Dickinson Park was the starting point for our drilling and is at an altitude of 3000 meters above sea level. The Dickinson Park is a quite isolated area of the national forest in the Wind River Range. Next to the park is the mire with the size of 0.8 square kilometers, which we investigate. The climate is characterized by semi-arid characteristics and steppe-like vegetation (Heidel, 2013). Since there is no climate data from Dickinson Park, the climatic data from Lander gives a briefly overview. The mean annual maximum temperature is 14.4° C and the mean annual minimum temperature is 0° C. Landers has a mean annual precipitation of 321 mm and a MAT of 7° C. (US Climate Data, 2009).

The park covers 5 kilometers of open parkland stretching north to south. The vegetation is countered by the confluent streams and the mire. Around the mire there are highland meadows and surrounded by forest. Despite its isolation, Dickinson Park is used by various groups of people. So the Dickson Park is the starting point for many hikes and in autumn hunters are on their way (Heidel, 2013).

The Wind River region, the largest mountain mass is in Wyoming, and Dickinson Park is in the middle of a center of one of the largest areas of Late Archean granitic bedrock in the Wind River Mountains (Heidel, 2013). Granodiorite and porphyritic and equigranular granite are the predominant granite bedrock. The lower located terrain, in contrast to the granites, are covered by sand, gravel and boulders eroded by the glaciers. The Wind River Range area has an extremely high density of wetlands (Copeland, et al., 2010). The area of the Wind River Range was in the past

strongly influenced by glaciers and the water from very large gel deposits is collected and forms Palustrine, riverine and lacustrine features (Heidel, 2013).

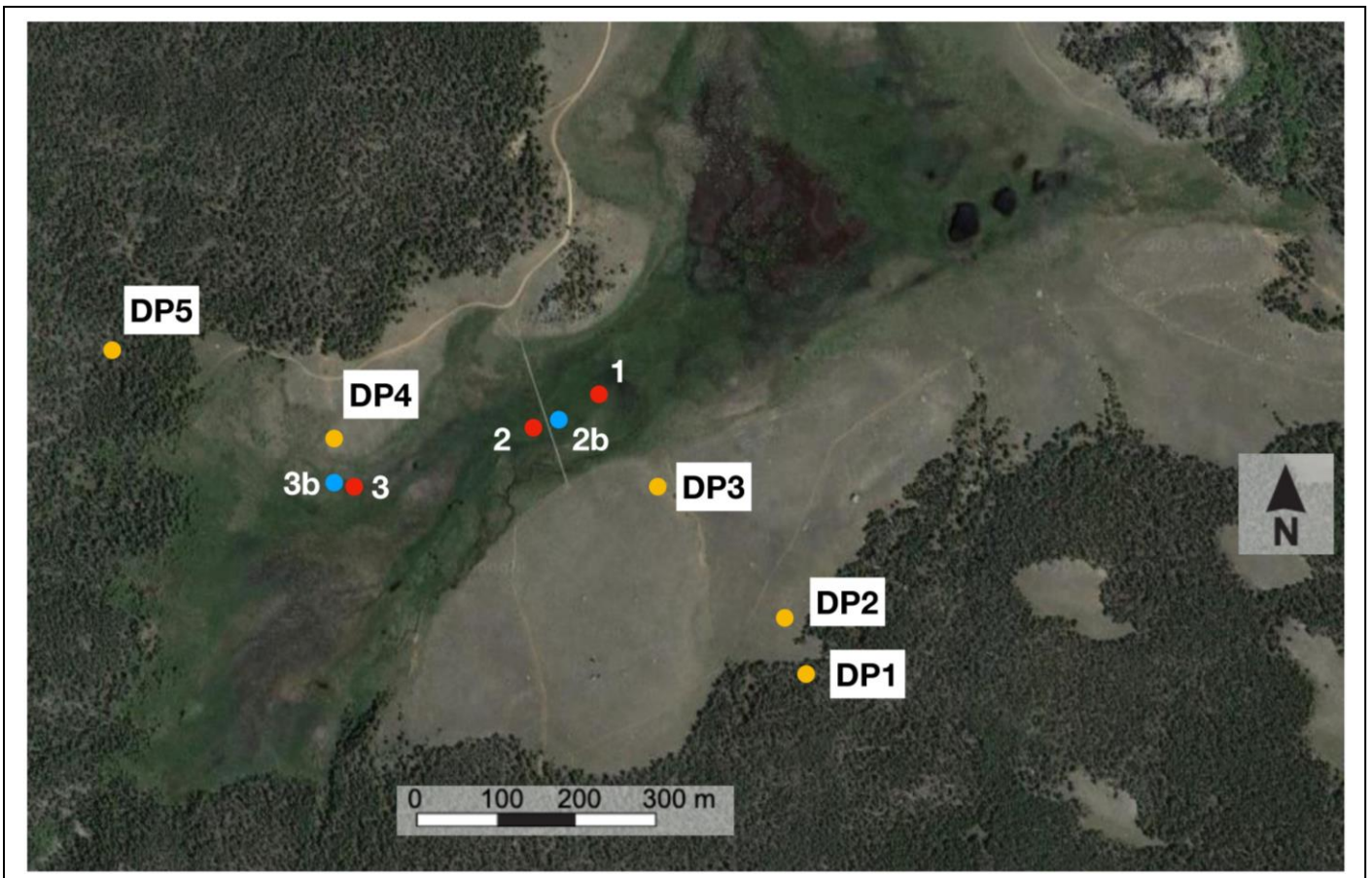


Figure 2: The map shows the soil profiles DP1-DP5 and the drill core profiles 1,2,3, 2b and 3b. DP is the abbreviation for the digged soil profiles and the numbers for the drilled mire profiles. The blue marked profiles are made in 2018, the red ones in 2017.

## 1.4 Mire and soil Samples

### 1.4.1 Sampling strategy and sample preparation

In 2018 two holes were made. Drilling was done using a VibraCore. The VibraCore consists of 4 elements. We have a drill head that is shaken by vibration in the ground. The head dodges inside the tube and so the soil material is transported into the tube. When the drill head is pulled out of the ground, the soil sample stays in the tube. By pushing the drill bit forward, the soil sample is squeezed out of the pipe and collected and packed in halved transport tubes. The second element of the Vibra Core are the extension rods. The drill head was able to secure one meter of soil material per pass. During the connection drilling, the extension bar was put on and the next meter could be drilled. So



we were able to drill to a depth of 6.5 meters. For this we needed three 2 meters extension rods and the drill head. The third element of the VirbaCor is the vibration motor, which is mounted on the drill head or on the extension rod. This vibration motor is powered by a generator and causes such a strong vibration on the drill head that it drifts into the ground. The last element of the VibraCore is a tripod with a pulley. This is needed to bring the drill head from the depth back to the surface. For every single hole, every meter, the whole VibraCore had to be disassembled and then rebuilt together. This resulted in the soil profile 2b and 3b.

After taking the soil samples, it was immediately packed in aluminum foil and dried immediately afterwards in the laboratory in the USA. During sampling, the cores were left in their entirety and not subdivided in depth. The division of the various drill cores into individual samples was first subdivided in the laboratory. The drill cores were dried at 40° C for 12 hours. This prevents the sample material from being changed. The dried material was then sent to Switzerland for further laboratory work.



*Picture 1 & 2: Field work at Dickison Park, Wind River Range, WY. In the left picture the installation of the vibration motor. In the right picture, the removal of the drill core with the help of the tripod.*

In addition, there was already sample material from the year 2017 from the same area. However, they could not drill deeper than 2 meters in 2017, because they did not have the right equipment for the mire. Also, 5 soil profiles were dug around the mire. Table 1-6 shows a list of all samples, including the five soil profiles.

#### 1.4.2 Sample preparation

The first processing step in Switzerland was to determine the skeletal portion of the samples and the fine earth fraction of the samples. Fine earth consists of material smaller than two millimeter and is relevant for further investigations regarding soil relevant physical and chemical parameters. The organic skeletal material was partially used for the later C14 study, but generally not further investigated. To determine the skeletal content and the fine soil, the material was processed with a hand sieve. Drying made the material extremely compact and strong, which is why a mortar was used. In addition, it was

important that the fine soil was absolutely homogeneous, because for the further analyzes partly smallest sample quantities were used. Part of the sieved sample material was also grounded.

## 2. Methods

### 2.1 Grain Size

With the particle size analysis can be given information about how the degree of weathering of the material is, and an estimation of the water and air balance of the soil is possible to made. In addition, the expandability, the exchange capacity, the nutrient content, but also the plastic properties of soils can be estimated (Rowell, 1994). The grain size analysis was made for the 5 soil profiles.

There is a large span of the grain size spectrum of a soil. In a first step, using a sieve analysis, the coarse fraction (gravel and sand) was separated in a range of 2000-31  $\mu\text{m}$  and then dried and weighed. Thus, the respective proportion of a grain size could be determined. Any material smaller than 32mm is defined as a fine fraction (silt or clay) and can be analyzed by its sedimentation rate. The rate of descent in a medium describes a function with which the density and grain size of the soil samples can be determined. For the rate of descent is, according to Stokes' law, a function of the density and viscosity of the falling medium, as well as the particle size and density of the sample material (Hiltmann & Stribny, 1998). The soil profiles (DP1- DP5) were examined more closely with the help of a wet sieving on the grain size. Sample material smaller than 32  $\mu\text{m}$  was measured with the X-Ray sedimentometer (SediGraph 5100).

### 2.2 pH

If one considers the sum of all ions in a soil solution, this is referred to as the electrolyte content, whereby one can characterize the concentration of these individually determined or in its entirety (Rowell, 1994). Of particular importance are the H and OH activities, which are constant at a certain temperature in aqueous solution, and usually only the H activity is measured.

An electrolytic solution ( $\text{CaCl}_2$ ) was used for the Ph measurement, so that the pH values are 0.3-0.8 lower than for a  $\text{H}_2\text{O}$  measurement (Schlichting, et al., 1995). The measurement with  $\text{CaCl}_2$  is more accurate and less susceptible to errors caused by the electrolyte concentration of the soil itself. The measurements are constant especially in soil samples, which the salt content fluctuates due to seasonal changes (Minasny, et al., 2011). A Ph meter was used for the measurement. Five grams of the soil samples were mixed together with 12.5 ml.

## 2.3 Atomic Absorption Spectrometry (AAS)

For the dried samples either oxalate or dithionite extracts were prepared. The aim of these extracts was to determine the iron, magnesium and aluminum concentration. The property of the solubility of oxides and hydroxides but also of selected silicates is used, which are different in different pretreatments. For both extracts, the solution is then measured using the AAS (Atomic Absorbance Spectrometry). The extract is atomized using a flame. A radiation source now sends rays through the atomized sample. Part of this sample absorbs the radiation source. Each element absorbs a certain wavelength. Then a detector detects on the other side the remaining radiation. The concentration of the individual elements can be determined by using the Beer- Lambert laws (Garcia & Baez, 2012).

### 2.3.2 Oxalate extraction

The oxalate extract dissolves amorphous and poorly crystallized Fe and Al phases in the soil. Also, disinfestations of ferrihydrite and allophane and imogolite are resolved and thus recorded in the extraction. In addition, phyllosilicates and interlayer silicates can also be partially detected by the oxalate extract (Walthert et al., 2004).

For the oxalate extract, 2 mg soil samples were shaken together with an ammonium and oxalic dihydrate solution for 2 h. It was important that the solution had a Ph value of 3. After the 2 hours, the liquid was filtered with a filter paper and then the measurement was made on the AAS.



*Picture 3: The soil samples shortly before they are filtered and then are already ready for AAS measurement.*

### 2.3.3 Dithionite extraction

In the dithionite extract, with the aid of sodium dithionite, which is a strong reducing agent, in addition to the organically bound Fe and Al, well-crystallized oxides and hydroxides are also dissolved. However, it is not possible to dissolve pedogenic oxides of aluminum. The reason for this is that the aluminum is not a redox sensitive element (Walthert, et al., 2004). Indeed, you would not like to attack the rock itself, so that in advance the Ph value must be buffered with NA carbonate, so that the Ph value is neutral (Egli, et al., 2018).

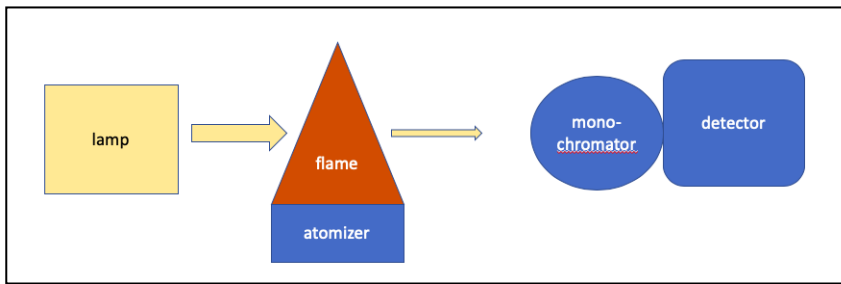


Figure 3: Schematic representation of the AAS measurement. The sample is atomized with the help of the atomizer and analyzed with the help of the radiation and the detector (according to Alfred Matthias, 2011).

To make a dithionite extract, one gram of the soil sample is heated with 8 ml sodium citrate solution and 2 ml sodium bicarbonate solution in a water bath. Then we added 1 g of sodium dithionite and left for 15 minutes in a water bath for 85 degrees. Then the solution is centrifuged and

the clear solution is decanted. The whole thing was completely made a second time with each sample. The mixture is then rinsed with a magnesium sulfate solution, centrifuged again and the clear liquid decanted. The clear liquid was then filled up with deion water and then the measurement was made on the AAS.

## 2.4 XRD

One way to examine soils for their mineral structure and expandability is by using the XRD method. This method is often applied to understand soil fertility, pedogenesis and various technical applications for soils (Aparicio, et al., 2010). For us, the study of different mineral structure was important. One of the most common techniques is X-ray powder diffraction. In the X-ray method, beams of different wavelengths of a radiation source are shot at the sample. This happens from different angles. Each mineral has its own reflective characteristics (Moore & Reynolds, 1997). However, certain mineral structures interfere with the reflection properties and it is therefore not always clear which mineral is present in the sample. This is why various minerals are modified with the help of various treatments, so that the reflection also changes and then it is clear which minerals are present in the samples (Aparicio, et al. 2010 and Moore & Reynolds, 1997).

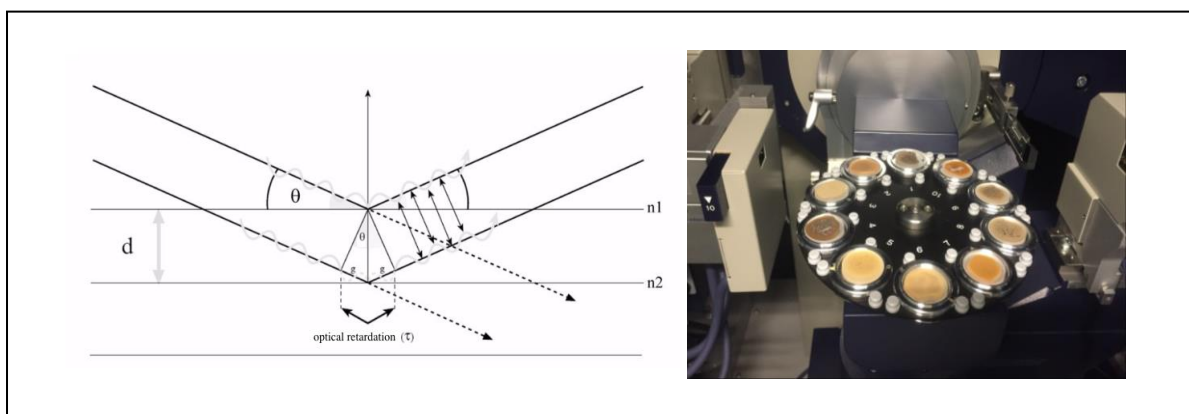


Illustration 1: On the left side the schematic representation of the XRD measurement (according to Moore & Reynolds, 1997). On the right side the samples in the XRD.

For this, the clay fraction must first be separated from the silk and sand fraction by means of a clay separation. Namely, the law of Stokes is used, according to which the smaller particles sink more slowly than the larger ones (Sathis Kumar & Naidu, 2011). First, organic material is destroyed with a Na acetate and then stirred the pH 5 buffered H<sub>2</sub>O<sub>2</sub> solution. After a certain time, the heavy parts sink and the suspension with the clay fraction is sucked off. The suspension is freeze-dried to subsequently obtain a powder with the clay fraction. For the actual measurements, so-called drip preparations as well as a powder preparation were used.

For the drip preparation the samples were saturated on the one hand with magnesium and on the other with potassium. For the drip preparation of the Mg saturated version, 25-30 mg of the clay fraction were mixed together with 2.5 ml NMgCl<sub>2</sub> and dissolved in a supersonic bath to give a suspension. Then the samples were centrifuged for 5 minutes to decant the supernatant. This process was repeated three times and then the sample was washed three times with 2.5 ml of H<sub>2</sub>O and the supernatant was decanted again. Then the sample was pipetted 1000-2000 µl on top of a glass plate. For the K saturated preparations, the pretreatment was the same, only that a KCl solution was used instead of the NMgCl<sub>2</sub> solution. Only with the MG saturated treatment, the distinguish between chlorite, smectite, vermiculite, hydroxy-interlayered smectite (HIS) and hydroxy-interlayered vermiculite (HIV) is not possible (Aparicio et al., 2010). The oriented soil samples are then applied to glass panes and subsequently analysed with X-rays. Cu-K $\alpha$  X-rays are used from 2 to 15°2 $\theta$  degrees in 0.02°2 $\theta$  steps per second. In addition, the samples were treated as follows: Mg saturation, glycerol saturation, and K saturation, additionally the samples were heated for 2 hours each to 335° and 550° degrees (Egli, et al., 2008).

The digitalized redness data were smoothed and corrected with the Lorentz and polarization factor. For peak separation and profile analysis we used the software Origin PFM™ where the Pearson VII algorithm was used. The program reconstructs all peaks and adjustments of the curve and the correction of overlapping peaks. In addition, there is the integral area as output, we also have the position of all individual peaks (Lanson, 1997).

Mineral	Treatment				HCl
	Air-dried	Glycol	Heated to 375°C	Heated to 550°C	
Illite	10	17	}	}	Insoluble
Glauconite Smectite (Na)					
Smectite (Ca, Mg) Illite-smectite	12*	17	}	}	Soluble Fe-rich species soluble
(random)	15*				
Illite-smectite	15-10*	Broad, higher orders non-integral 15-10	}	}	Insoluble
(ordered)		Higher orders non-integral unless near 50:50			
Kaolinite, dicke Chlorite (Fe-rich)	7.15	7.15	7.15	Destroyed	}
	14.2	14.2	14.2	14.2 Enhanced	
Berthierine Chlorite (Mg-rich)	7	7	Often sensitive	Destroyed	}
	14.1	14.1	14.1	14.1 Enhanced	
Corrensite	28	31 Integral higher orders	24	12	}
Chlorite (dioctahedral)	14.1	14.1	14.1	14.1 Enhanced	
Tosudite	28	31 Integral higher orders	24	12	}
	*Function of relative humidity				

Table 1: This table shows the effect of different treatments on the basal spacing of some clay minerals.

### 2.4.1 Clay minerals and their response to the various treatments

Mg saturated smectite shows a peak based on 1.5 nm series and then expands after EG solvation to 1.7 nm. K saturated smectite produce a series based on 1.25 nm and collapse to 1 nm after heating up to 550 C (Moore & Reynolds, 1997 & Hillier, 2003). The Vermiculites create a peak around 1.4nm after the Mg Saturation, this peak collapse by the k saturation to 1 nm (Moore & Reynolds, 1997). With the EG treatment the peaks can expand between 1.4 to 1.6 nm (Moore & Reynolds, 1997). Illite is a quite resist clay mineral, which have a serie of peaks around 1 nm and this peak are not modified by any treatments (Hillier, 2003). If we still have a peak after heating the sample to 550° C we know the we have chlorite in our sample, because smectic and vermiculites collapse by this high temperature to 1 nm. After heating the kalium-saturated samples to 335 degrees, HIV collapse to 1 nm (Hillier, 2003 & Moore & Reynolds, 1997).

## 2.5 X-Ray Fluorescence (XRF)

The XRF method can be used to determine the complete elemental composition of a soil sample. In this process, the single atoms are excited by X-rays, so that the electrons are removed from the near-core orbit and are ionized. Electrons from higher orbitals replaced the ionized electron. In this process, fluorescent X-rays are emitted. For the stabilization of the atom, it is based on the fact that the electron of a shell closer to the nucleus is more strongly bound to the nucleus. In this case, the binding force of the atomic number  $Z$  is determined, which defines the energy level of the individual shells and thus ultimately the fluorescence radiation which is defined by its energy difference. This fluorescence X-ray is relatively low in interference, meaning that there is little overlay and the appearance of fluorescence lines of different elements at similar energy levels (Alfeld, 2016).

For our samples, 5g of finely ground samples were filled into small plastic containers which have a special foil. This special foil does not disturb the X-rays and also not the fluorescence X-rays. Thereafter, the measurement is carried out on the XRF device itself.

## 2.6 Diffuse Reflectance Infrared Fourier Transformation (Drift)

The DRIFT method uses infrared radiation to determine the clay minerals and organic substances in a soil sample. This measurement method is simple and very fast (Zimmermann, et al., 2011). Infrared light is focused on a sample from a thermal source. Part of this radiation from being reflected off the surface, another part of the radiation can penetrate into the sample, gets scattered there and then exits again if it is not absorbed (Egli, et al., 2018). This leaked radiation is recorded in a very large solid angle by a detector. In this process, the infrared radiation takes two separate paths in the measurement. On the one hand, the infrared radiation passes directly to the detector, and on the other hand, the reflected radiation is detected by the detector. Due to the difference of the measurement an interferogram can be created. This interferogram gives information about different clay minerals in our sample (Egli, et al., 2018).

In the measurements, 30 mg of soil samples weighing 270 mg KBr each were weighed into an Eppendorf tube. Then will heat the sample to 105 degrees for 2 hours. The typical peaks for quartz is around 780 and 800  $\text{cm}^{-1}$ , the peaks for kaolinite 3694 and 3622  $\text{cm}^{-1}$  and the peak of 3624 and 531 is attributed to mica (Boxleitner, et al., 2017). Imogolite type material shows a peak at 3620, 3526, 3469  $\text{cm}^{-1}$  and gibbsite around 1017  $\text{cm}^{-1}$  (Boxleitner, et al., 2017). For the peak analyses I used the OPUS 6.5 software.

## 2.7 Loss of Ignition (LOI)

To measure the organic content in a soil sample, the LOI method is used (Smith, 2003). In this case, the heating of the samples burns the organic portion of the sample and thus the proportion can be determined. For this purpose, 2 g of soil samples were placed in crucible. These crucibles were then heated at 550 degrees for 6 hours. Subsequently, the sample was weighed again and the difference of the weight gives the proportion of the organic material.

## 2.8 Total Carbon Content - Combusting Method

The CHN instrument can diagnose carbon, hydrogen and nitrogen. This is done by high temperatures, where these elements are separated from the material. This happens in an oxygen-rich environment. The result of this combustion is CO<sub>2</sub>, H<sub>2</sub>O N<sub>2</sub> and SO<sub>x</sub>. These gases are detected by different processes and thus one can measure C, H and N elements (Egli, et al., 2018).

For preparation, 0.2 mg of ground soil samples are filled in a very thin capsule. The capsule must be folded into a small ball, possible without any edges.

## 2.9 C14

One of the core measurements for this master's thesis was the age determination of mire and sediment samples. Similarly to Boxleitner et al. (2017), peat samples and samples having organic remains were cleaned using an acid-alkali-acid (AAA) treatment. The samples were then heated under vacuum in quartz tubes with CuO (oxygen source) to remove any absorbed CO<sub>2</sub> in the CuO. The tubes were evacuated again, sealed and heated in the oven at 900 °C to obtain CO<sub>2</sub>. The CO<sub>2</sub> of the combusted sample was mixed with H<sub>2</sub> (1:2.5) and catalytically reduced over iron powder at 535 °C to elemental carbon (graphite). After reduction, the mixture is pressed into a target and carbon ratios was measured by Accelerator Mass Spectrometry (AMS) using 0.2 MV radiocarbon dating facility (MICADAS) of the Ion Beam Physics at the Swiss Federal Institute of Technology Zurich (ETHZ). The calendar ages were obtained using the OxCal 4.3 calibration program (Bronk Ramsey, 2001-2009) based on the IntCal 13 calibration curve (Reimer, et al., 2013). Calibrated ages are given in the 2  $\sigma$  range (minimum and maximum value for each). Age-depth modelling was performed using the R-code 'clam' (Blaauw, 2010). When 14-C ages are reported, then the age indication is given in cal (k)a BP. More general age indications (not or not purely related to <sup>14</sup>C) are given as (k)a BP)



### 3. Results

The mire near Dickson Park is located next to a large moraine and is therefore related to this landform. Cosmogenic nuclide dating ( $^{10}\text{Be}$ ) revealed ages between 537 and 17.8 ka (Table 1) when using a rock surface erosion of 1 mm per ky<sup>-1</sup>. With 2 mm erosion per ky<sup>-1</sup>, the ages varied between 160.9 ka and 17.8 ka. These ages therefore indicate deposits from MIS 2 to MIS 14 etc. This moraine is consequently composed of several glacial deposits.

Unit / Sample #		Lat (°N)	Long (°W)	Elevation (m a.s.l.)	Sample thickness (cm)	Shielding factor	Erosion rate (mm ky <sup>-1</sup> )	10Be content (x10 <sup>5</sup> atoms g <sup>-1</sup> )	<sup>10</sup> Be Exp Age (ka)
<b>Dickinson Park</b>	DIP-1	42,824	-109,056	2880	2,0	0,997	1,00	113.44 ± 2.53	<b>537.7 ± 97.7 (28.1)</b>
	<i>WRRR</i> DIP-2	42,825	-109,056	2882	2,0	0,999	1,00	116.42 ± 2.33	<b>560.4 ± 104.4 (27.6)</b>
	DIP-3	42,828	-109,0452	2870	2,0	0,998	1,00	42.84 ± 0.86	<b>138.2 ± 15.3 (3.6)</b>
	DIP-4	42,827	-109,04101	2873	2,0	0,997	1,00	41.85 ± 0.84	<b>134.4 ± 14.8 (3.4)</b>
	DIP-5	42,824	-109,04427	2901	2,0	1,000	1,00	46.76 ± 1.03	<b>149.8 ± 16.9 (4.3)</b>
	DIP-6	42,825	-109,03647	2913	2,0	0,998	1,00	17.63 ± 0.41	<b>51.1 ± 5.2 (1.3)</b>
	DIP-7	42,824	-109,03682	2919	2,0	1,000	1,00	6.89 ± 0.20	<b>20.0 ± 2.0 (0.6)</b>
	DIP-8	42,822	-109,03989	2929	2,0	0,852	1,00	5.25 ± 0.17	<b>17.8 ± 1.8 {0.6}</b>
Unit / Sample #		Lat (°N)	Long (°W)	Elevation (m a.s.l.)	Sample thickness (cm)	Shielding factor	Erosion rate (mm ky <sup>-1</sup> )	10Be content (x10 <sup>5</sup> atoms g <sup>-1</sup> )	<sup>10</sup> Be Exp Age (ka)
<b>Dickinson Park</b>	DIP-1	42,824	-109,056	2880	2,0	0,997	<b>2,00</b>	113.44 ± 2.53	<b>saturated</b>
	<i>WRRR</i> DIP-2	42,825	-109,056	2882	2,0	0,999	<b>2,00</b>	116.42 ± 2.33	<b>saturated</b>
	DIP-3	42,828	-109,0452	2870	2,0	0,998	<b>2,00</b>	42.84 ± 0.86	<b>160.9 ± 21.2 (5.1)</b>
	DIP-4	42,827	-109,04101	2873	2,0	0,997	<b>2,00</b>	41.85 ± 0.84	<b>155.4 ± 20.2 (4.8)</b>
	DIP-5	42,824	-109,04427	2901	2,0	1,000	<b>2,00</b>	46.76 ± 1.03	<b>176.7 ± 24.2 (6.3)</b>
	DIP-6	42,825	-109,03647	2913	2,0	0,998	1,00	17.63 ± 0.41	<b>51.1 ± 5.2 (1.3)</b>
	DIP-7	42,824	-109,03682	2919	2,0	1,000	1,00	6.89 ± 0.20	<b>20.0 ± 2.0 (0.6)</b>
	DIP-8	42,822	-109,03989	2929	2,0	0,852	1,00	5.25 ± 0.17	<b>17.8 ± 1.8 {0.6}</b>

Table 2: The following table shows the results of the beryllium measurement. In a first calculation the erosion rate was 1mm per<sup>-1</sup>. In a second calculation the erosion rate was adjusted to 2mm.

### 3.1 Soils

The soils around the mire developed on moraine deposits and on colluvial slope materials, from the surrounding mountains. Profile DP5 and DP1 are located in the surrounding forests of the mire. DP3 and DP4 are located close to the mires and DP2 slightly further away. The soil profiles have a typical structure with an A horizon followed by the Bw horizon and finally a Cox or BC horizon. The Ph value generally decreases in all soil profiles with the depth. All five soil profiles have a C<sub>org</sub> proportion between 4.5% and 9% in the topsoil. Organic matter strongly decreases with depth (Table 4). This is also reflected in the LOI content.

Among other things, the DRIFT analysis reflects the granite source material. We find quartz and mica in all of our samples (Table 3). Dolomite can be found in almost all horizons. Kaolinite is found in all horizons. Chlorite could only be detected in soil profiles DP3 and DP4. There we also detected gibbsite. The Oxalate results show, that Al and Mn have their lowest values in the mother soils and increase in the topsoils in the oxide form. This is also the case everywhere with Fe, except for the soil profile DP5. There the Fe content in the bottomsoil increases strongly.

Sample	Horizon	Kaolinite	Gibbsite	Quartz	Mica	Calcite	Dolomite	Chlorite
DP1	A	x	(x)	x		(x)	x	
	Bw	x		x	x	(x)	x	
	Bc	x		x	x	(x)	x	
DP2	A	x			x	(x)	x	
	Bw1	x			x	(x)	x	
	Cox	x			x	(x)	x	
DP3	A	x	x		x	x	x	x
	Cox	x	x		x	x	(x)	x
DP4	A	x	(x)			x		
	2Bc	(x)		x			(x)	(x)

Table 3: The DRIFT results of the soil profile DP1-DP5

Locality	Elevation feet (meters)	Horizon Horizon Depth (cm)	Horizon thickness	Gravel >2mm (g)	Fine earth <2mm (g)	GRAV %	Vol % grav	% CaCO <sub>3</sub> HCL	pH	Al(o) mg/kg	Mn (o) mg/kg	Fe(o) mg/kg	Si(o) mg/kg	N (%)	C (%)	C/N	LOI (%)	
								Sand (2-0.5 mm)										
DP1-1	2886	A	0-0	10	27	436	6	2	50	4,55	4773	1314	5969	488	0,25	4,50	17,95	13,3
DP1-2		Bw1	10-30	20	201	346	37	22	50	4,25	3402	97	5428	361	0,07	0,92	13,95	6,1
DP1-3		Bw2	30-85	55	489	254	66	57	84	4,38	2216	70	1334	378	0,07	0,18	2,60	2,2
DP1-4		Cox	85+	15	597	288	67	59	84	4,50	1688	164	1347	233	0,01	0,14	13,03	2,1
DP2-1	2870	A	0-2	2	129	249	34	19	59	5,31	1855	511	4239	270	0,53	7,10	13,49	16,9
DP2-2		BA	2-15	13	119	385	24	17	62	4,92	2031	247	4398	550	0,28	3,08	11,07	9,0
DP2-3		Bw1	15-30	15	229	433	35	28	68	4,50	2034	31	3013	359	0,13	1,33	10,36	5,7
DP2-4		Bw2	30-53	23	272	416	39	31	70	4,30	1694	68	3478	204	0,05	0,63	11,92	4,8
DP2-5		Bt	53-60	7	237	455	34	29	77	4,21	1048	65	1551	93	0,02	0,28	14,89	2,6
DP2-6		Cox	60+	40	239	345	41	36	71	4,24	627	43	895	65	0,01	0,17	13,21	1,8
DP3-1	2858	A	0-10	10	111	362	24	12	53	5,30	1835	309	3036	389	0,43	4,89	11,49	12,2
DP3-2		Bw	10-25	15	209	314	40	27	66	4,94	1995	138	1834	332	0,18	2,11	11,96	6,2
DP3-3		BC	25-45	20	180	324	36	29	71	4,79	1363	61	1076	216	0,10	1,20	12,56	4,3
DP3-4		Cox	45+	55	341	448	43	37	80	4,92	326	31	304	36	0,01	0,18	13,15	0,9
DP4-1	2865	A	0-7	7	142	390	27	13	55	5,31	1488	497	3016	238	0,54	6,36	11,72	13,2
DP4-2		AB	7-20	13	264	439	38	23	56	4,95	1529	387	2373	1259	0,18	2,01	11,00	6,0
DP4-3		2Bw	20-45	25	583	375	61	47	78	5,07	820	39	593	43	0,07	0,42	6,38	4,6
DP4-4		2BC	45+	55	220	526	30	20	72	4,97	745	54	313	29	0,04	0,80	21,82	5,7
DP5-1	2883	OA	0-4	4	39	371	9	3	51	4,92	1745	616	2925	423	0,40	8,95	22,18	19,7
DP5-2		Bw	4-20	16	123	548	18	11	70	4,51	783	12	2801	87	0,03	0,53	15,33	3,4
DP5-3		2Bg	20-90	70	18	551	3	1	43	4,52	1241	5	3234	231	0,04	0,49	11,62	6,1
DP5-4		2CBg	90-100+	30	208	596	26	21	67	4,84	771	54	4174	236	0,02	0,30	15,16	3,9

Table 4: Here are the most important soil data of the soil profile DP1-DP5.

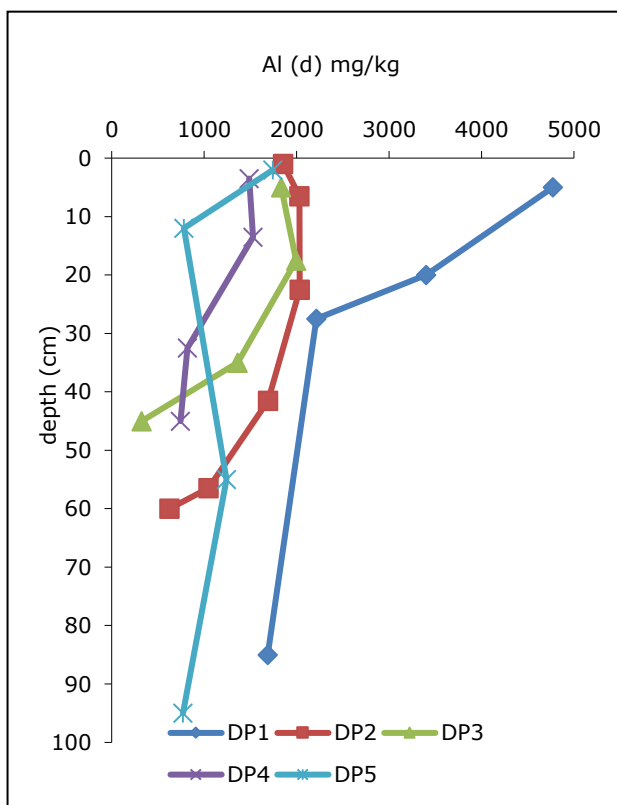
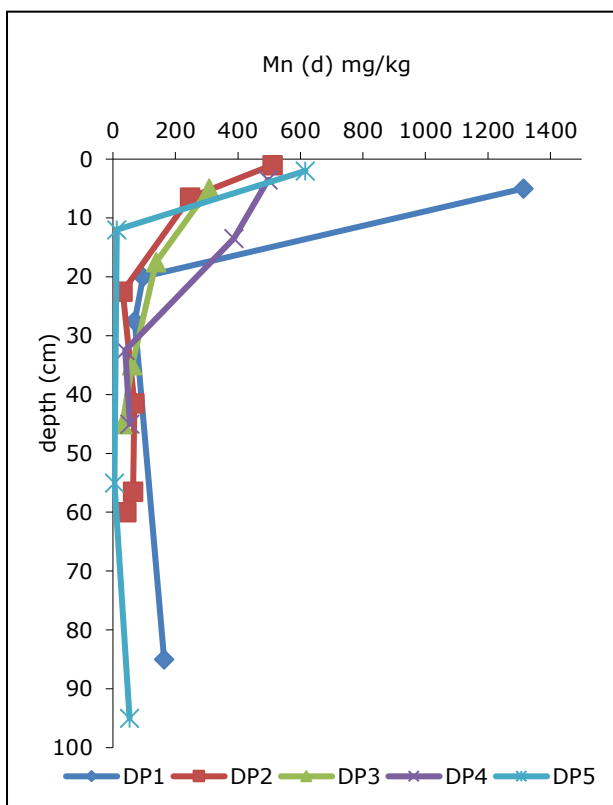
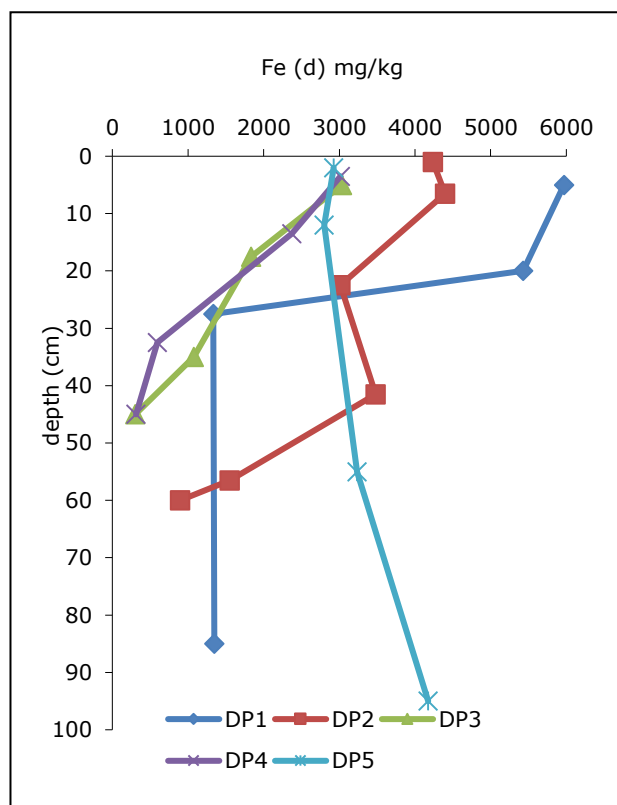
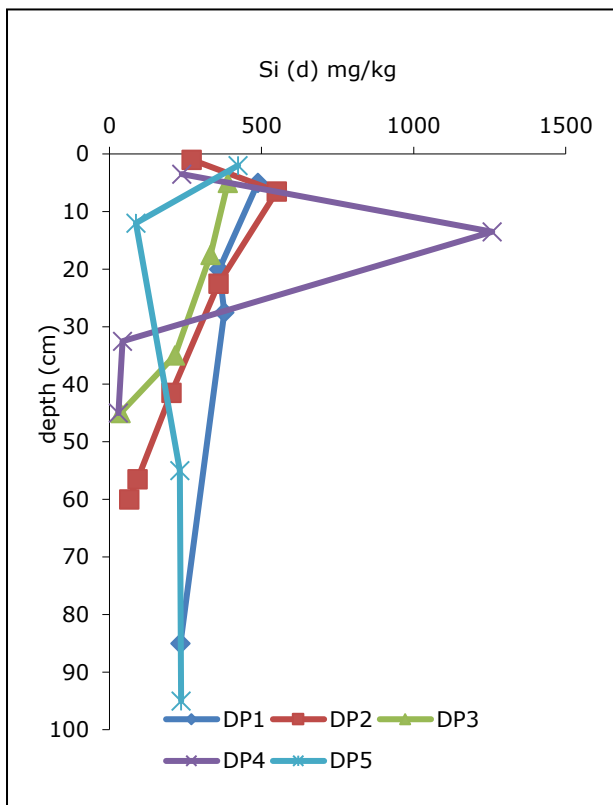


Figure 4: The dithionite extracts of the soil profiles DP1-DP5

### 3.1.2 Dithionite Extraction of the soils

If observing the dithionite extracts (Figure 4) with the respective elements, one can clearly see that the soil profile DP1, which is located east of the moor, initially has the highest values. The curve of Mn and Al is very similar for all profiles. Especially DP2-5 behave very the same with Al, white also on the surface almost an identical value. With the depth the Mn value decreases and goes down to 0 in almost all profiles. At the Si value DP4 has a strong outlier in a depth of 15 cm.

With the Fe values the profiles run very differently. DP1,2,3 and 4 the Fe value decreases with depth. With DP 5, on the other hand, the value increases.

### 3.1.3 Clay Minerals of the soils

#### XRD measurements

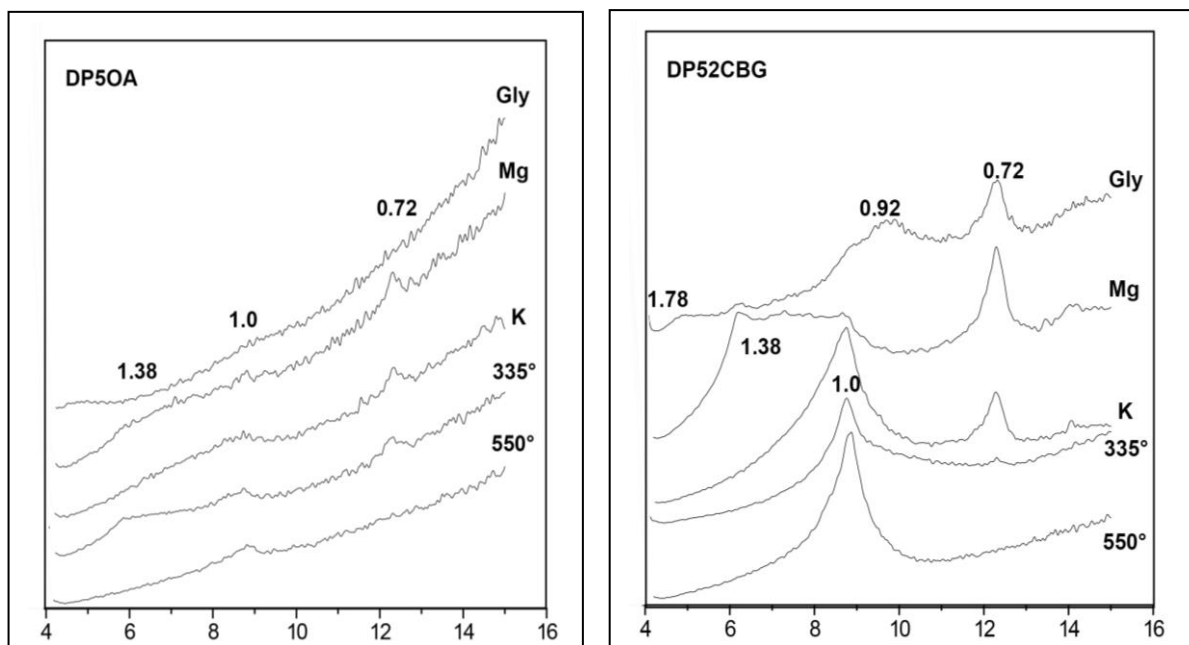


Figure 5: X ray-patterns of the XRD measurement of the soil profile DP5. d-spacing are given in nm. Mg=Ma saturation, Gly= ethylene glycol solvation, K0 K saturation and corresponding heating treatments.

The XRD measurements were only partially successful. Measurements were made of all soil profiles from the top horizon and the bottom horizon. The lower soil horizons all look very good and important information can be read. But the upper horizons were only partially readable.

Kaolinite is present in all horizons, which can be seen at the peak of 0.72. Mica can't be detected, but there should have been a peak at 1.0 and 0.33 nm. Chlorites are not found in any samples. In DP2Cox, the 1.41nm shifts slightly, which could also lead to smectite closure. Because the peak of 1.4 collapses

to 1.00nm at potassium saturation. The same happens with the DP5 profile. Smectic and vermiculite are also present here. There is a peak at 1.4nm in the magnesium saturated sample which collapses to 1nm in the potassium saturated sample. However, there is only little Smectic available. The two profiles DP2 and DP5 do not differ very much from each other, although they are far away and on the other side of the mire. In DP5 as well as in DP2 there is little Illite, this can be seen at the peak by 1nm, which gets smaller, but remains the same during all treatments. In DP2 Cox the vermiculite is clearly visible. HIV also collapses at 550 degrees, as can be seen with DP2Cox. There the peak becomes even higher at 550 degrees, which can be an indication that there is HIV in the sample.

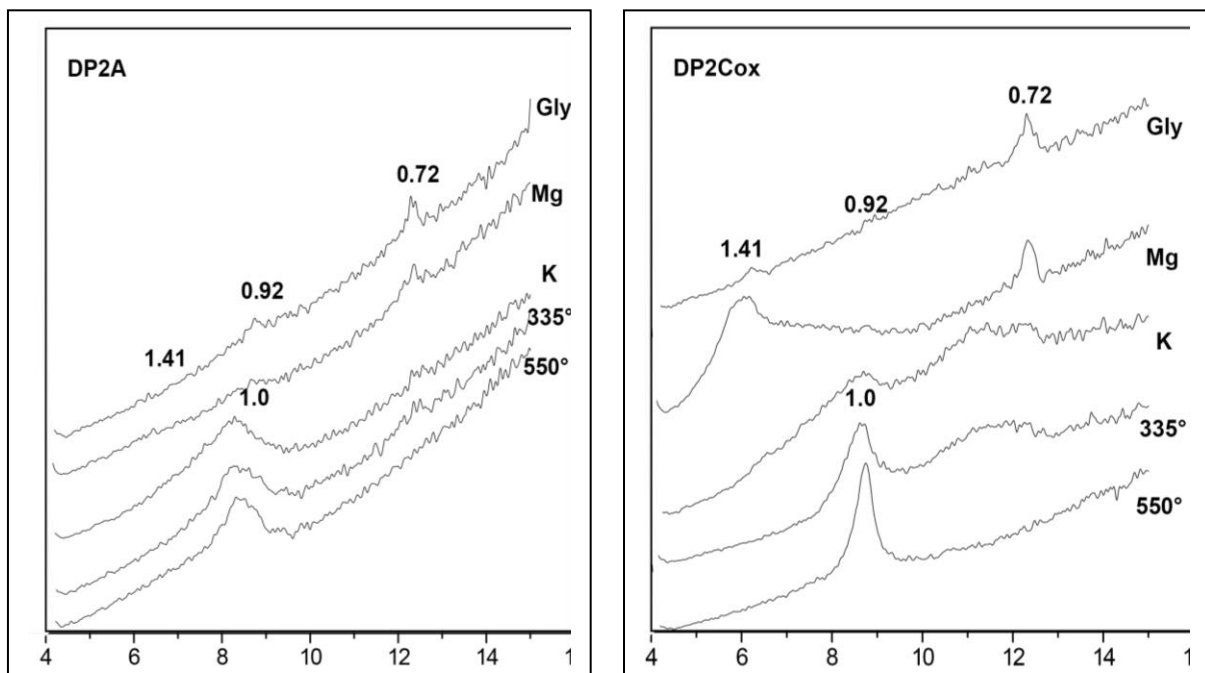


Figure 6: X ray-patterns of the XRD measurement of the soil profile DP2. d-spacing are given in nm. Mg=Ma saturation, Gly= ethylene glycol solvation, K0 K saturation and corresponding heating treatments.

Locality /profile	Sample	Depth(cm)	Skeleton content (%)	LOI (%)	pH (CaCl2)	Bulk density (g/cm3)
profile 2b, on the eastern side of the bridge						
	S2_1	100-110	5,59	24,0	4,28	1,20
	S2_2	110-120	14,41	50,0	4,52	0,51
	S2_3	120-130	29,95	5,6	4,29	1,56
	S2_4	130-140	21,26	29,0	4,42	0,79
	S2_5	140-150	28,71	3,1	4,38	1,46
	S2_6	150-160	37,70	3,0	4,39	1,64
	S2_7	160-170	30,01	1,4	4,6	1,97
	S2_8	170-180	10,91	1,0	4,31	1,75
	S2_9	180-190	37,03	1,8	4,05	2,32
	S2_10	190-200	34,66	1,4	4,02	1,62
	S2_11	200-210	39,20	3,9	4,12	4,12
	S2_12	210-220	42,43	3,0	4,11	4,20
	S2_13	220-230	23,32	1,8	4,49	1,86
	S2_14	230-240	28,08	1,3	4,3	1,52
	S2_15	240-250	37,40	1,6	4,02	1,37
	S2_16	250-260	41,09	2,3	3,91	2,78
	S2_17	260-270	41,70	2,3	4,3	1,08
	S2_18	270-280	14,60	1,1	4,49	0,94
	S2_19	280-290	25,37	1,1	4,44	1,42
	S2_20	290-300	31,29	1,2	4,55	1,37
	S2_21	300-310	19,99	1,7	4,27	1,05
	S2_22	310-320	39,07	0,9	4,22	1,24
	S2_23	320-330	44,60	1,1	4,11	0,80
	S2_24	330-340	37,38	1,0	4,1	1,30
	S2_26	350-360	46,12	1,9	4,05	1,40
	S2_27	360-370	39,22	2,0	4	1,69
	S2_28	370-378	46,20	1,9	3,95	0,81

Table 6: Profile 2b, located next to the bridge.

Locality /profile	Sample	Depth(cm)	Skeleton content (%)	LOI (%)	pH (CaCl2)	Bulk density (g/cm3)
profile 2, on the western side of the bridge						
	R2_12	0-11	5,4	44,5	4,17	0,28
	R2_1	11-23	27,7	1,5	4,4	
	R2_22	23-35	4,5	17,2	4,23	0,63
	R2_2	35-50	5,1	1,4	4,31	
	R_32	50-63	3,0	16,1	4,23	0,98
	R2_3	63-75	3,5	1,6	4,34	
	R2_42	75-90	2,3	27,0	4,31	0,93
	R2_4	90-102	8,8	0,8	4,43	
	R2_52	102-115	1,5	33,8	4,52	0,36
	R2_5	115-125	37,8	2,6	-	
	R2_62	125-144	3	23,2	4,52	0,67

Table 5: Profile 2, which was drilled in 2018



## 3. 2 Mire Cores

### 3.2.1 pH, LOI & Bulk density

Looking at the pH values of the 5 profiles, one can see a clear trend. Profile 3 and 3b have a higher pH value than the others. In addition, the pH value increases in depth at profile 3b. The bulk density (Figure 8) of all five profiles are very similar in the first meter and are between 0.2 and 1.5g/cm<sup>3</sup>. In addition, profile 2b and profile 3b clearly show an outlier of density at around 2 meters depth. Over the entire profile, the bulk density varies strongly. No trend in bulk density can be detected, but the range of bulk density remains the same and is always between 3 and 0.2g/cm<sup>3</sup>.

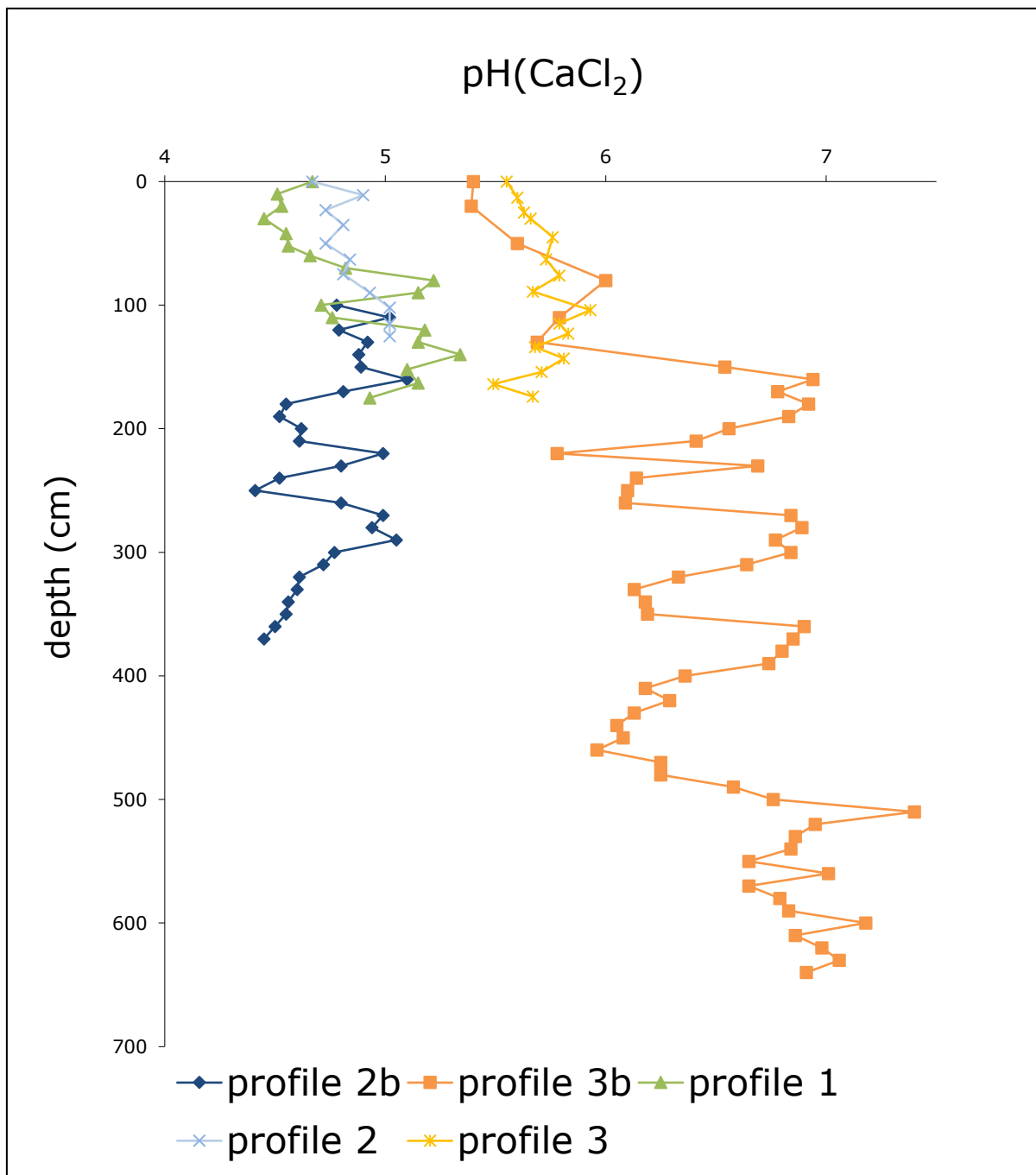


Figure 7: pH values of all mire cores

Locality /profil	Sample	Depth(cm)	Skeleton content (%)	LOI (%)	pH (CaCl2)	Bulk density (g/cm3)
<b>profil 3b, in the middle of the western part of the mirer</b>						
S3_1	0-20		19,40	77,2	4,9	0,22
S3_2	20-50		9,40	70,7	4,89	0,27
S3_3	50-80		2,30	71,7	5,1	0,40
S3_4	80-110		2,40	69,7	5,5	0,55
S3_5	110-130		5,60	44,0	5,29	0,81
S3_6	130-150		5,32	44,4	5,19	0,09
S3_7	150-160		37,20	3,2	6,04	1,73
S3_8	160-170		47,10	2,3	6,44	0,72
S3_9	170-180		65,53	2,1	6,28	1,34
S3_10	180-190		61,60	2,2	6,42	1,87
S3_11	190-200		46,28	1,6	6,33	2,69
S3_12	200-210		31,20	2,4	6,06	2,08
S3_13	210-220		51,20	2,8	5,91	1,74
S3_14	220-230		41,41	2,7	5,28	1,73
S3_15	230-240		45,70	3,2	6,19	2,09
S3_16	240-250		39,92	2,2	5,64	1,51
S3_17	250-260		50,90	1,7	5,6	1,64
S3_18	260-270		45,80	1,1	5,59	0,73
S3_19	270-280		39,60	4,6	6,34	1,17
S3_20	280-290		41,40	2,5	6,39	1,38
S3_21	290-300		59,40	2,1	6,27	2,05
S3_22	300-310		41,45	2,1	6,34	1,80
S3_23	310-320		39,80	2,3	6,14	0,64
S3_24	320-330		60,80	2,5	5,83	1,11
S3_25	330-340		51,38	2,0	5,63	1,25
S3_26	340-350		58,00	2,7	5,68	1,05
S3_27	350-360		43,93	2,7	5,69	0,64
S3_28	360-370		32,80	3,9	6,4	1,09
S3_29	370-380		43,04	8,3	6,35	1,84
S3_30	380-390		34,70	3,7	6,3	1,94
S3_31	390-400		35,56	3,1	6,24	2,05
S3_32	400-410		56,70	2,4	5,86	1,60
S3_33	410-420		59,46	2,6	5,68	1,54
S3_34	420-430		31,90	3,4	5,79	1,50
S3_35	430-440		33,95	2,9	5,63	0,98
S3_36	440-450		52,90	3,1	5,55	0,96
S3_37	450-460		40,10	2,8	5,58	0,79
S3_38	460-470		37,80	1,5	5,46	1,00
S3_39	470-480		35,20	2,0	5,75	1,54
S3_40	480-490		51,27	1,8	5,75	1,23
S3_41	490-500		58,90	2,1	6,08	1,53
S3_42	500-510		56,20	2,4	6,26	0,73
S3_43	510-520		57,24	2,9	6,9	1,28
S3_44	520-530		27,60	3,7	6,45	1,81

Table 7: Mire Cores 1, 3 and 3b with the values of LOI, skeleton content, pH and Bulk density

Locality /profil	Sample	Depth(cm)	Skeleton content (%)	LOI (%)	pH (CaCl2)	Bulk density (g/cm3)
<b>profile 3b, in the middle of the western part of the mirer</b>						
S3_45	530-540		23,30	3,9	6,36	1,72
S3_46	540-550		35,35	5,7	6,34	1,72
S3_47	550-560		2,80	1,9	6,15	1,02
S3_48	560-570		14,20	1,6	6,51	1,19
S3_49	570-580		37,68	1,5	6,15	1,41
S3_50	580-590		46,30	1,8	6,29	0,74
S3_51	590-600		42,81	3,1	6,33	1,33
S3_52	600-610		40,20	2,2	6,68	0,79
S3_53	610-620		30,77	3,9	6,36	0,90
S3_54	620-630		30,00	5,0	6,48	0,86
S3_55	630-640		46,00	2,7	6,56	0,55
S3_56	640-648		75,22	3,0	6,41	0,81

Locality /profil	Sample	Depth(cm)	Skeleton content (%)	LOI (%)	pH (CaCl2)	Bulk density (g/cm3)
<b>profile 1, on the eastern side of the bridge</b>						
R1_1	0-10		17,9	1,22184209	4,17	
R1_12	10-20		15		4,4	0,29
R1_2	20-30		19,4	1,13311819	4,03	
R1_22	30-42		2		1,9	0,66
R1_3	42-52		20,3	0,2228282	4,05	
R1_32	52-60		1		9	1,46
R1_4	60-70		19,4	0,55159481	4,16	
R1_42	70-80		2,8		2,09	0,85
R1_5	80-90		20,3	3,04624891	4,72	
R1_52	90-100		4,9		3,2	0,53
R1_6	100-110		17,8	0,77453428	4,21	
R1_62	110-120		1,7		1,95	0,91
R1_7	120-130		19,3	3,71997287	4,68	
R1_72	130-140		0,9		5,6	0,48
R1_8	140-152		3,7	1,892699	4,84	
R1_82	152-163		0,7		4,21	0,42
R1_9	163-175		9	1,67307037	4,65	
R1_92	175-189		5,2		2,3	0,88
<b>profile 3, in the middle of the western part</b>						
R3_1	0-12		27,6		4,08	0,15
R3_12	13-25		0		71,20	5,1
R3_2	25-35		14,4		4,40	5,13
R3_22	30-45		0		74,50	5,16
R3_3	45-57		6,2		4,42	5,26
R3_32	63-71		0		65,40	5,23
R3_4	76-89		7,3		1,69	5,29
R3_42	89-104		0		39,30	5,17
R3_5	104-114		39,9		3,35	5,43
R3_52	115-123		0		27,30	5,29
R3_6	123-133		38,2		2,43	5,33
R3_62	134-143		0		53,10	5,18
R3_7	143-153		4,1		2,55	5,31
R3_72	154-164		0		32,90	5,21
R3_8	164-174		32,8		2,69	4,99
R3_82	174-184		0		43,00	5,17

The same depth trend like the pH can also be seen for the LOI as a function of the profile. Again, it is noticeable that the values of the profiles 3 and 3b differ significantly the other three locations. In the upper layers, the LOI at Profile 3 and 3b are almost 80 %. Profile 1 and profile 2 only have a value of around 40 % there. At a depth of 180 cm and lower, the LOI percentage is very low.

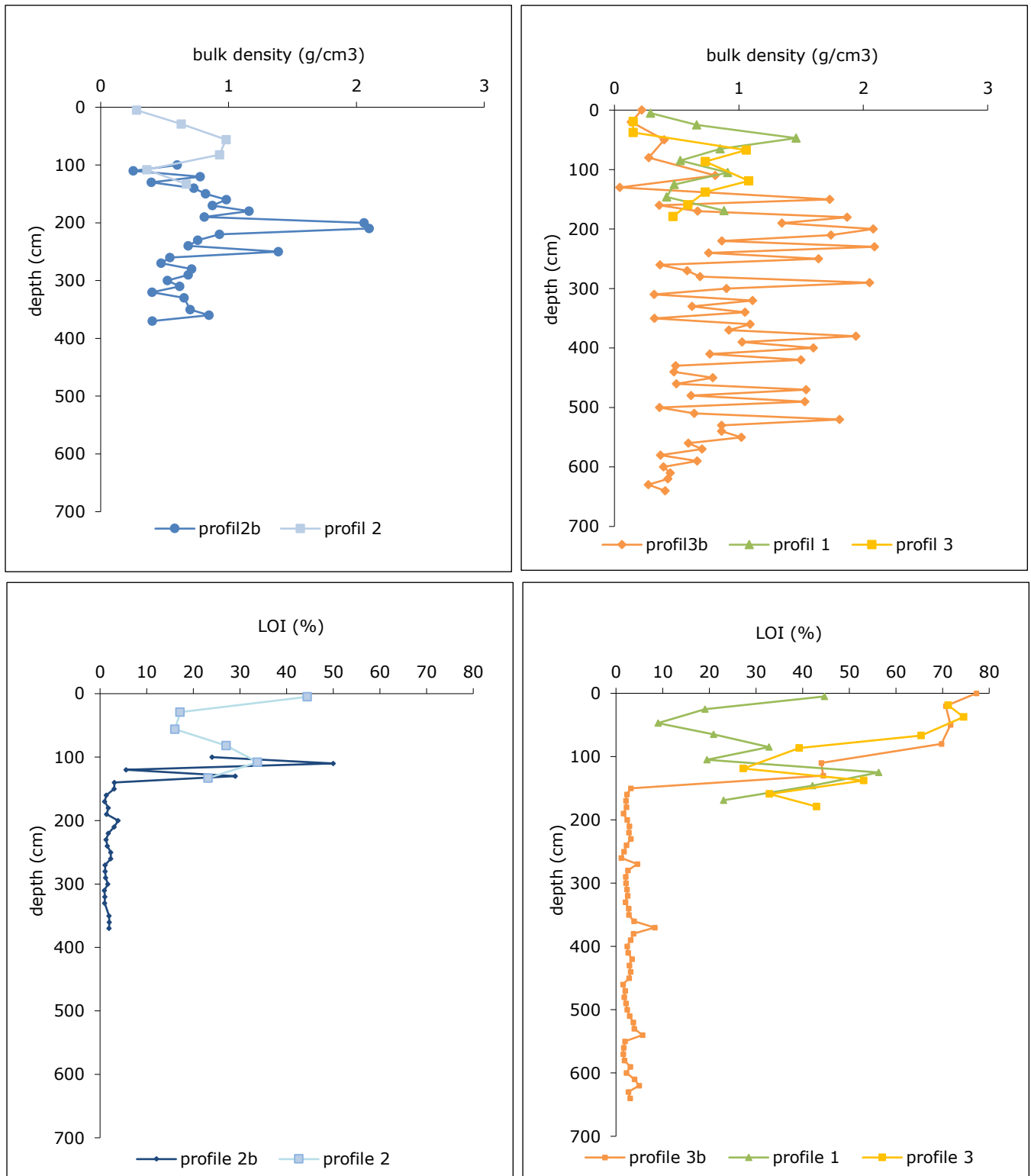


Figure 8: LOI and Bulk Density values for the profile 1,2+2b,3 and 3b

Site	Depth	Kaolinite	Gibbsite	Quartz	Mica	Chlorite	Imogolite	okt. Mg/Fe	Smectic
Profil 3b	10	x		(x)					x
	65	x		(x)	x				x
	120	x	(x)	x	x		x		x
	155	x		(x)					x
	185	x		x					
	205	x	(x)	x	x				x
	215	x		x	(x)				
	235	x	x	x	x		(x)		
	255	x	x	x					
	295	x	x	x	x				
	325		x	x	x				
	345	x		x	x				
	365	(x)		x			x		
	385			x	x				
	405	x	(x)	x	(x)		(x)		(x)
	425	x		x	x		x		
	455	x		x	x		x		
	475	x	(x)	x	x		x		
495		(x)	x			x			
525		(x)		x		(x)			

Site	Depth(cm)	Kaolinite	Gibbsite	Quartz	Mica	Chlorite	Imogolite	okt. Mg/Fe	Smectic
Profil 1	5	x		x	x		(x)	x	
	25	x		x	x	(x)	x	x	
	47	x	(x)	x	x	(x)	x	x	
	65	x	(x)	x	x		(x)	x	
	85	x		x	x		(x)	x	
	105	x	(x)	x	x	(x)	(x)		
	125	x	(x)	x	x		(x)		
	146	x		x	x			x	
	169	(x)		x	x			x	
Profil 2	5			x	x		(x)		
	29		(x)	x	x		(x)		
	56	x		x	x				
	82	x		x	x				
	108	x		x	x		(x)		
	133	x		x	x			x	
Profil 3	19	(x)		(x)	x				
	37	(x)	(x)	x	x		(x)		
	67	x	(x)	x	x		(x)		
	86	x	(x)	x	x		(x)	x	
	119	x		x	(x)				
	138	x		x	x		(x)		
	159	x		x	x		x		
	179	x	(x)	x					

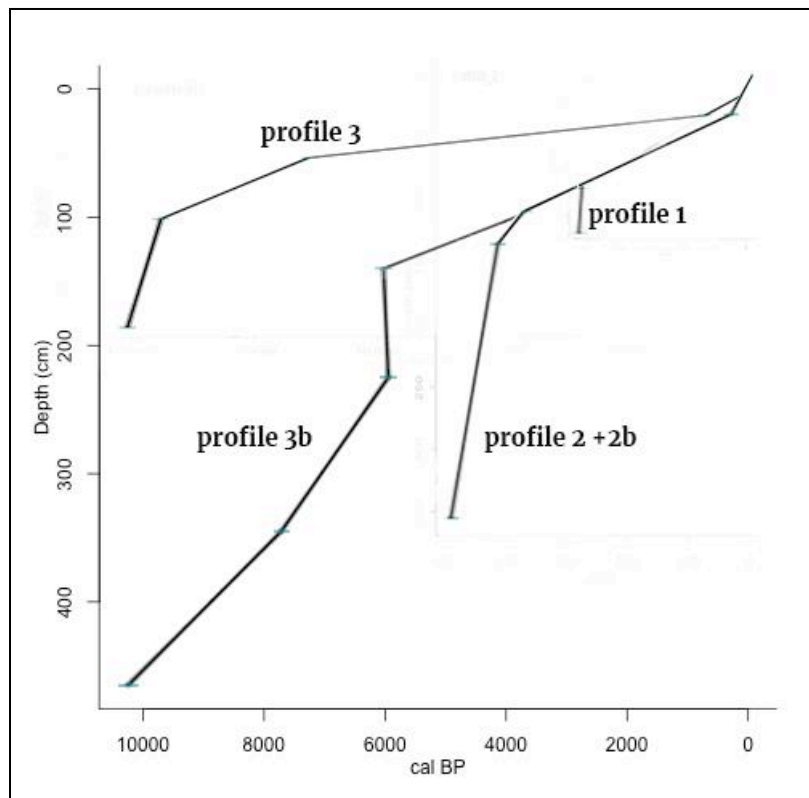
Table 8: An overview of the DRIFT results of profiles 1,2,3 and 3b.

### 3.2.2 C14 Dating of the mire deposits

A total of 14 soil samples were successfully dated. A maximum age of 10245 – 10188 calBP was reached at a depth of 465 cm in profile 3b. The complete age sequence is given in Table . The youngest age measured was 90 years in profile 1 at a depth of 15 cm. The ages of profiles 1, 2+2b and 3b are similar down to a depth of one meter. Only profile 3 has already from 20 cm completely different age trend. In general, it can be seen that the age trends of profiles 3 and 3b are similar, although they seem “displaced”. Profile 1 and 2, but also profile 3b, show a clear change at 1 meter and at 1.5 m, respectively.

Unlike the pH values, there are no such clear differences in age between the profile sites. Although the age-depth trend has a similar shape, it seems shifted in time; e.g., with profile 3 an age of 10210 – 9917 calBP is already reached at a depth of 179 cm. At 3b we reach a comparable age at a depth of 450 cm. If we look at profiles 1 and 2, there is a strong change between the years 3500 and 4100. For profile 3b, this change only occurs in the year 6000.

Based on the age trends, a sedimentation rate per year was calculated. The sedimentation rate increased strongly with age for profiles 1 and 2+2b (Figure 20) For all profiles the sedimentation rate starts between 0 and 0.1 cm per year. At profile 1, the sedimentation rate increases strongly at 2000 years to



0.7 cm per year. For profiles 2 + 2b the sedimentation rate also accelerates strongly, but with a delay around 4000 calBP. The sedimentation rates for profiles 3 and 3b are lower than for the other two profiles. Although there is also an increase with age, the values do not exceed 1 cm per year. Here, too, a locality trend can be seen in the sedimentation rate. The sedimentation rates of 3 and 3b are very similar to those of the other profiles.

Figure 9: All age depths Trend of all profiles compiled in one diagram.

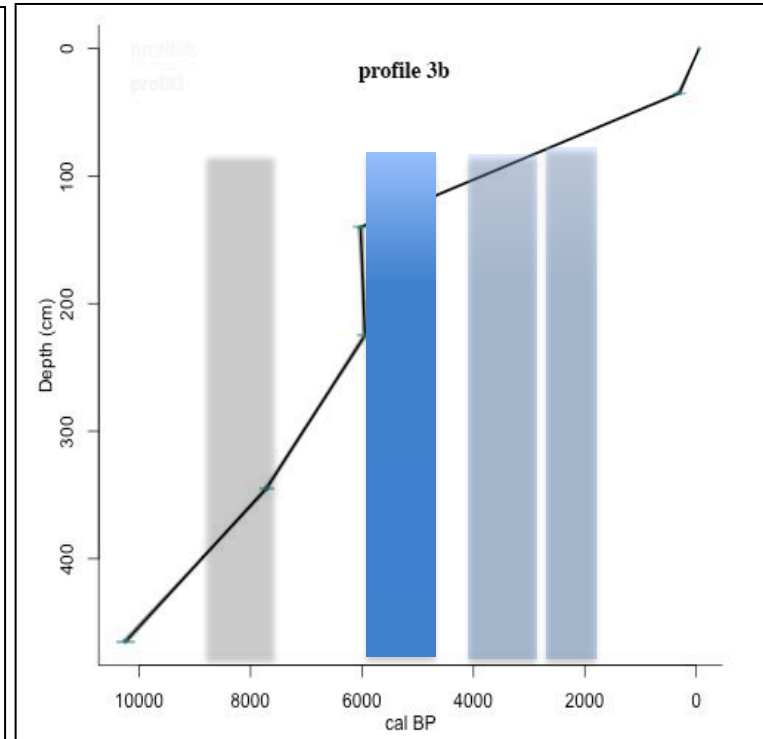
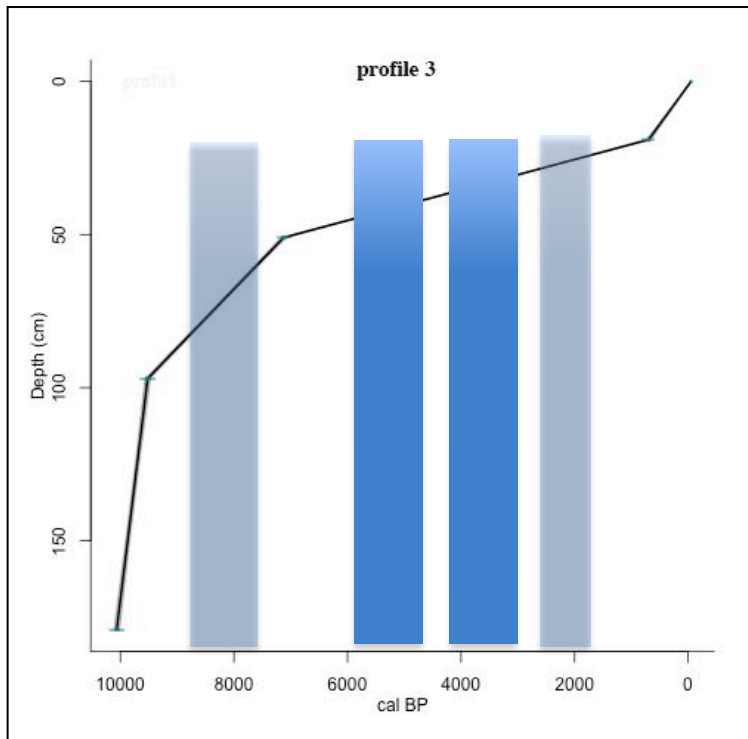
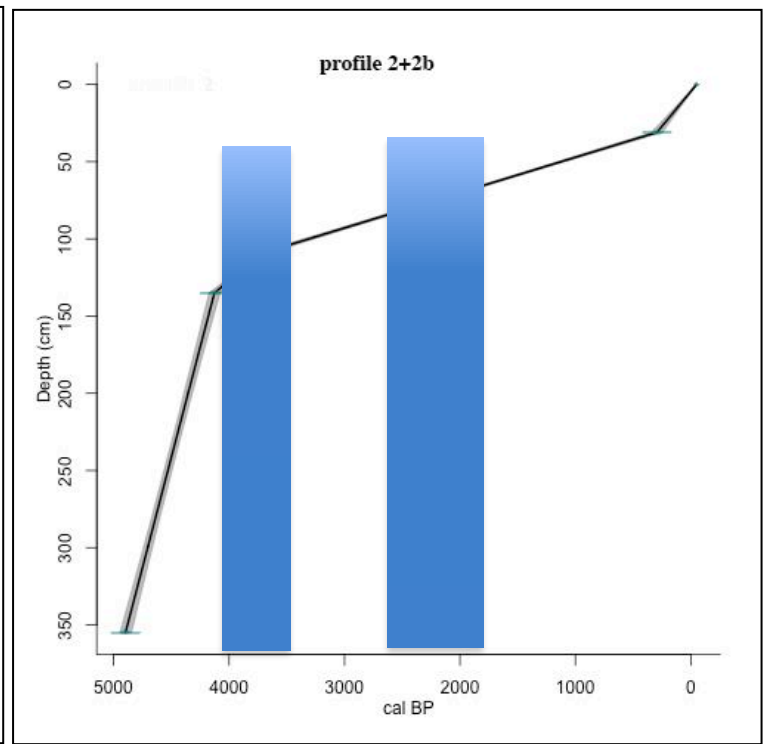
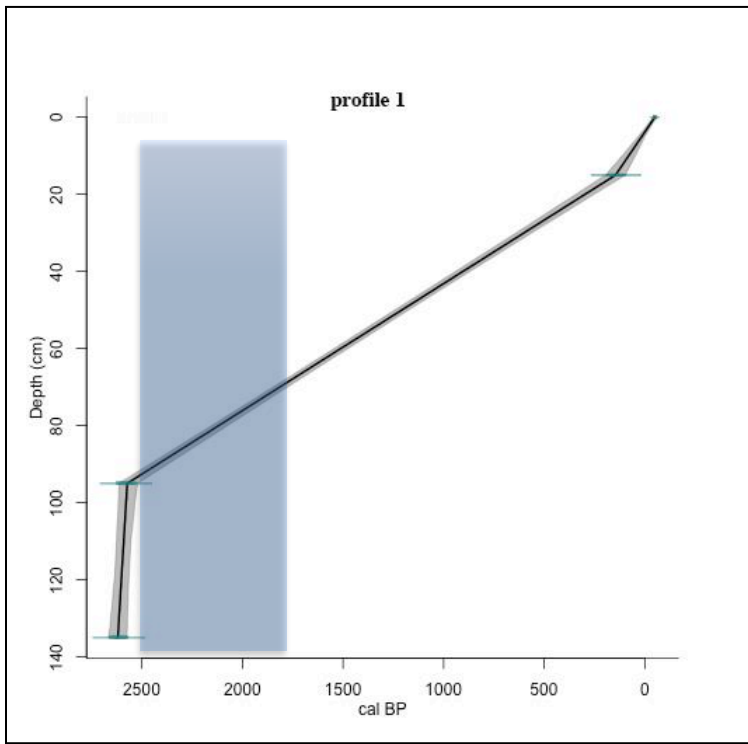


Figure 10: The four diagrams show the age depth trend of the profiles 1, 2+2b, 3 and 3b and in blue the cold periods.

	Sample-Nr.	Sample Code	Description	Code-Nr.	Material	C14 age BP	±1σ	F14C	±1σ	δC13	±1σ	Calibrated ages (2-sigma) calBP
Profile 1	ETH-84317	6471	Wind River Range	Profil 1_10-20	peat	90	25	0,9888	0,0031	-37,1	1	260 - 25
	ETH-84318	6472	Wind River Range	Profil 1_90-100	peat	2478	26	0,7346	0,0024	-29,9	1	2720 - 2437
	ETH-84319	6473	Wind River Range	Profil 1_130-140	peat	2509	26	0,7318	0,0024	-30,3	1	2738 - 2490
Profile 2 + 2b	ETH-84321	6475	Wind River Range	Profil 2_23-35	peat	273	25	0,9666	0,003	-27,4	1	430 - 155
	ETH-84322	6476	Wind River Range	Profil 2_102-115	peat	3418	28	0,6535	0,0023	-27,6	1	3819 - 3584
	ETH-94376	6499	Wind River Range	S2_2*	organic matter	2773	23	0,7081	0,0020	-26,3	1	2994 - 2792
	ETH-84323	6477	Wind River Range	Profil 2_125-144	peat	3776	29	0,625	0,0022	-26,2	1	4241 - 4010
	ETH-94378	6501	Wind River Range	S2_26*	organic matter	4311	25	0,5847	0,0018	-24,5	1	4960 - 4836
Profile 3	ETH-84324	6478	Wind River Range	Profil 3_13-25	peat	753	26	0,9105	0,0029	-28,5	1	727 - 666
	ETH-96755	6513	Wind River Range	Core 3 R#3-3	organic matter	6211	27	0,4616	0,0016	-23,9	1	7241 - 7009
	ETH-96756	6514	Wind River Range	Core 3 R#3-4	organic matter	9018	31	0,3254	0,0013	-29,8	1	10237 - 10175
	ETH-84325	6479	Wind River Range	Profil 3_89-104	peat	8553	38	0,3448	0,0016	-27,1	1	9555 - 9482
	ETH-84326	6480	Wind River Range	Profil 3_174-184	peat	8944	39	0,3284	0,0016	-27,3	1	10210 - 9917
Profile 3b	ETH-94379	6502	Wind River Range	S3_2*	organic matter	223	22	0,9726	0,0026	-27,5	1	307 - 0
	ETH-94380	6503	Wind River Range	S3_6*	organic matter	5243	27	0,5206	0,0017	-28,8	1	6175 - 5923
	ETH-94381	6504	Wind River Range	S3_14*	organic matter	5150	26	0,5267	0,0017	-32,5	1	5987 - 5766
	ETH-96753	6511	Wind River Range	S3_24	organic matter	4992	27	0,5372	0,0018	-32,4	1	5880 - 5650
	ETH-96754	6512	Wind River Range	S3_26	organic matter	6834	28	0,4271	0,0015	-31,5	1	7716 - 7608
	ETH-94384	6507	Wind River Range	S3_38*	organic matter	9049	32	0,3242	0,0013	-30,3	1	10245 - 10188

Table 9: Here are all the results of the C14 measurements. A total of 16 measurements were executed. These measurements themselves were made at the ETH, the preparations at the University of Zurich.

### 3.2.3 Elemental contents of the mire

#### Total contents and weathering indices

##### Total content of Al, Fe and Si

What can be clearly seen is that the Si content, both in profile 2b and in profile 3b, increases with age. The aluminum content of both profiles remains constant between 8 and 10%. Up to 6000 years the Si and Al content of profile 3b increases continuously, after which many small disturbances occur. In profiles 2+2b, the Al and Si content remains stable up to 4000 years, after that the content changes and varies strongly. In profile 1, both the Si and Al content rapidly decreased 2000 years ago, followed by a strong increase after about 2500 years. The two trends for Al and Si are almost parallel for the cores 1 and 3. The values of the cores 3 and 1 are very different. Core 3 and 3b have similar trends, but core 3b has a “delay” of about 2000 years. Profile 2+2b are similar to profile 1 as far as the range of values is concerned. Especially at a depth of 100 cm similar fluctuations can be seen for Al. With Si we are in the same range, but the amplitudes are different.

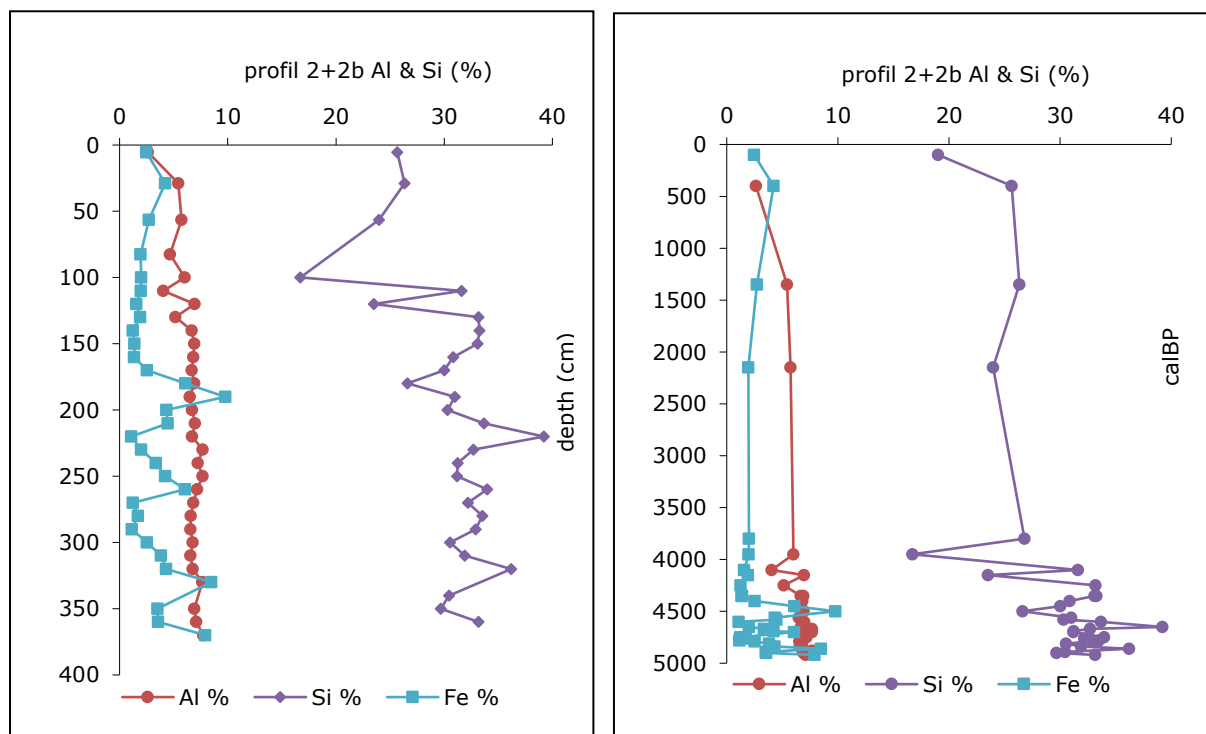


Figure 11: The Al, Si and Fe percentage of the profile 2+2b.



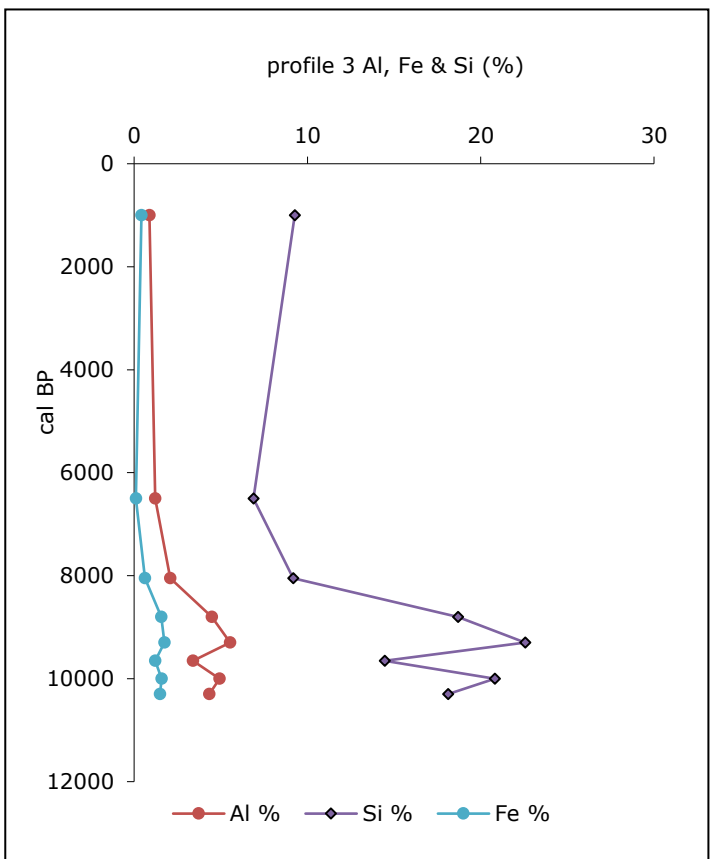
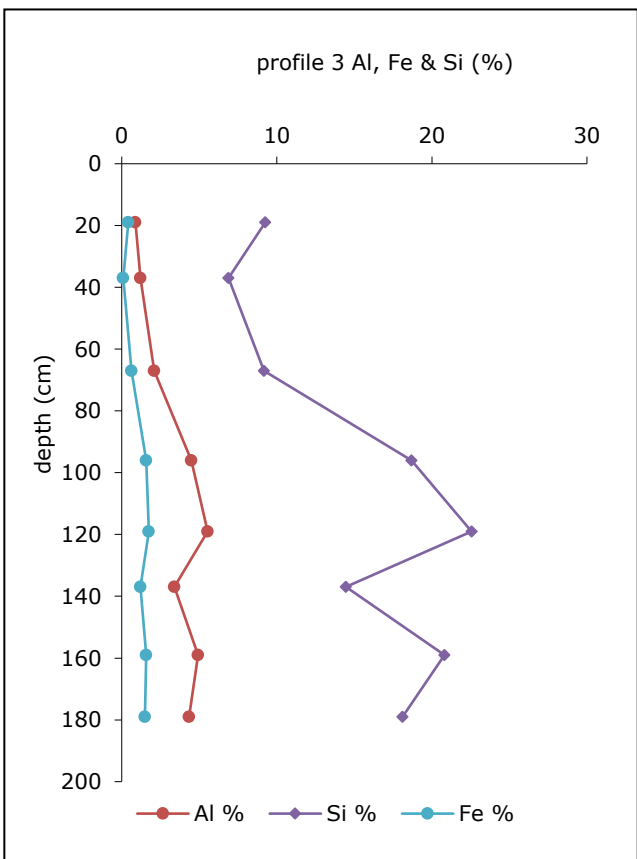
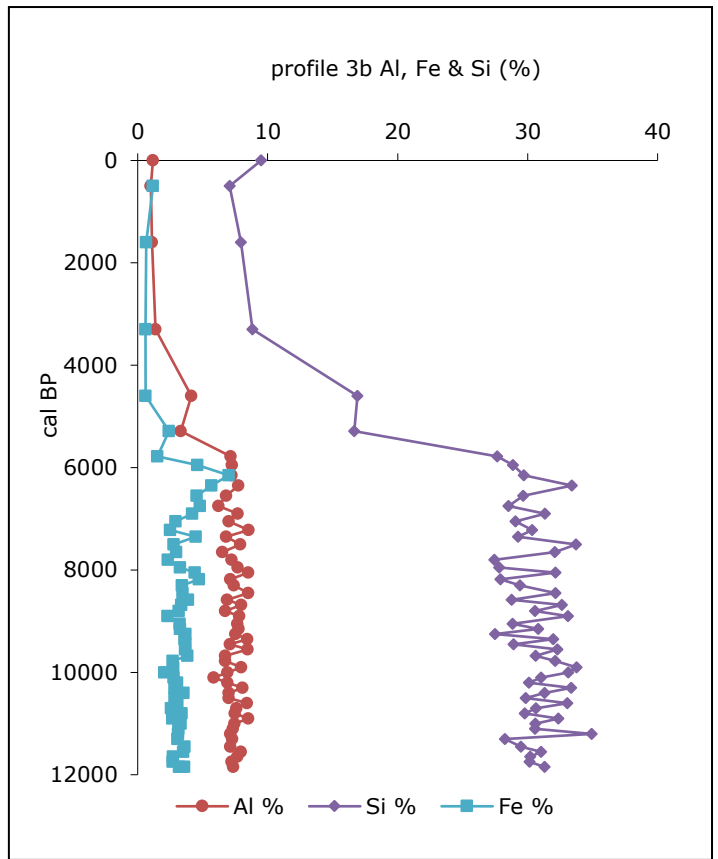
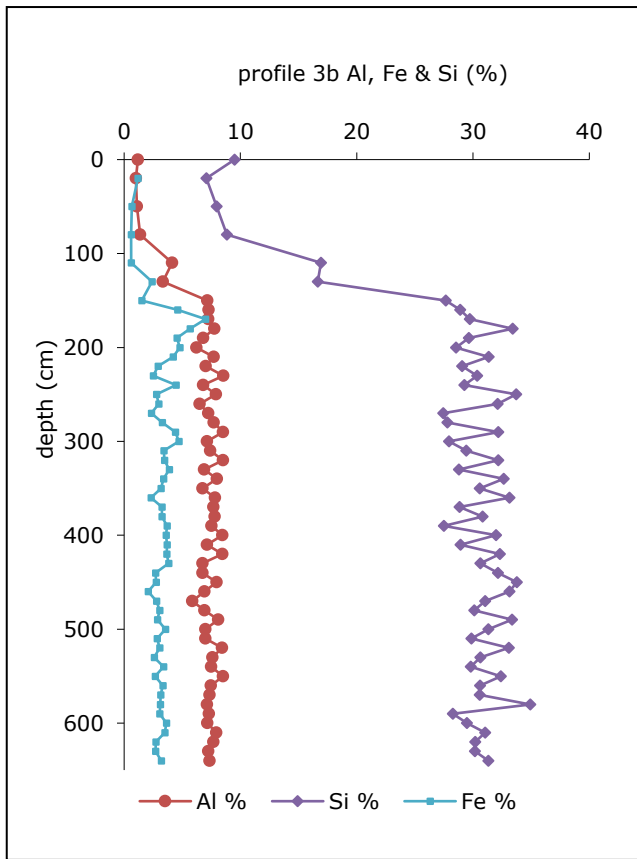


Figure 12: The four diagrams show the Al, Fe and Si content in percent of profiles 3 and 3b, displayed once as depth function and once as age function.

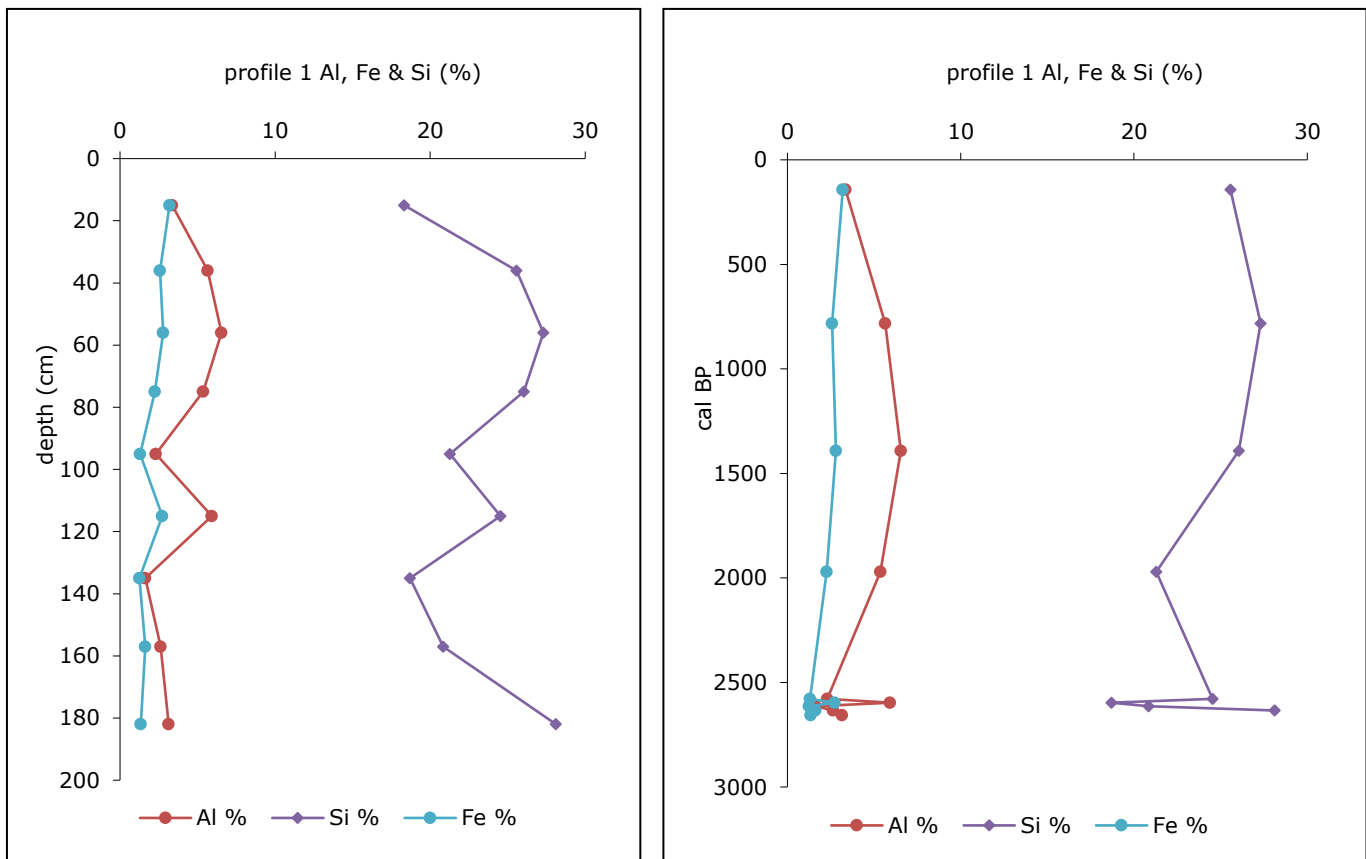


Figure 13: The two diagrams show the Al, Fe and Si content in percent of profiles 1, displayed once as depth function and once as age function.

If we look at the Fe value, a noticeable increase around 4500 years BP can be detected in profiles 2+2b. This is not the case in the other drilling cores. Only for profile 3b, there is a similar increase for 6000 years. This deflection is also almost the same and goes up to almost 10 percent for profile 3b and over 10 percent for profile 2+2b.

#### Oxalate extractable contents

The Mn content varies significantly between profile 3b and 2+2b. If the Mn content in profile 3b is high, it is lower in profile 2+2b and vice versa. In addition, the Mn content increases substantially from 6000 calBP in profile 3b. However, the Fe content is higher in profile 2+2b than in profile 3b. The Al content of profile 2+2b is comparable to profile 3b. About 4000 and 6000 calBP, respectively, the Al content in both profiles decreases strongly. From a depth of 2 meters on, strong fluctuations can be seen in profiles 3 and 3b,.

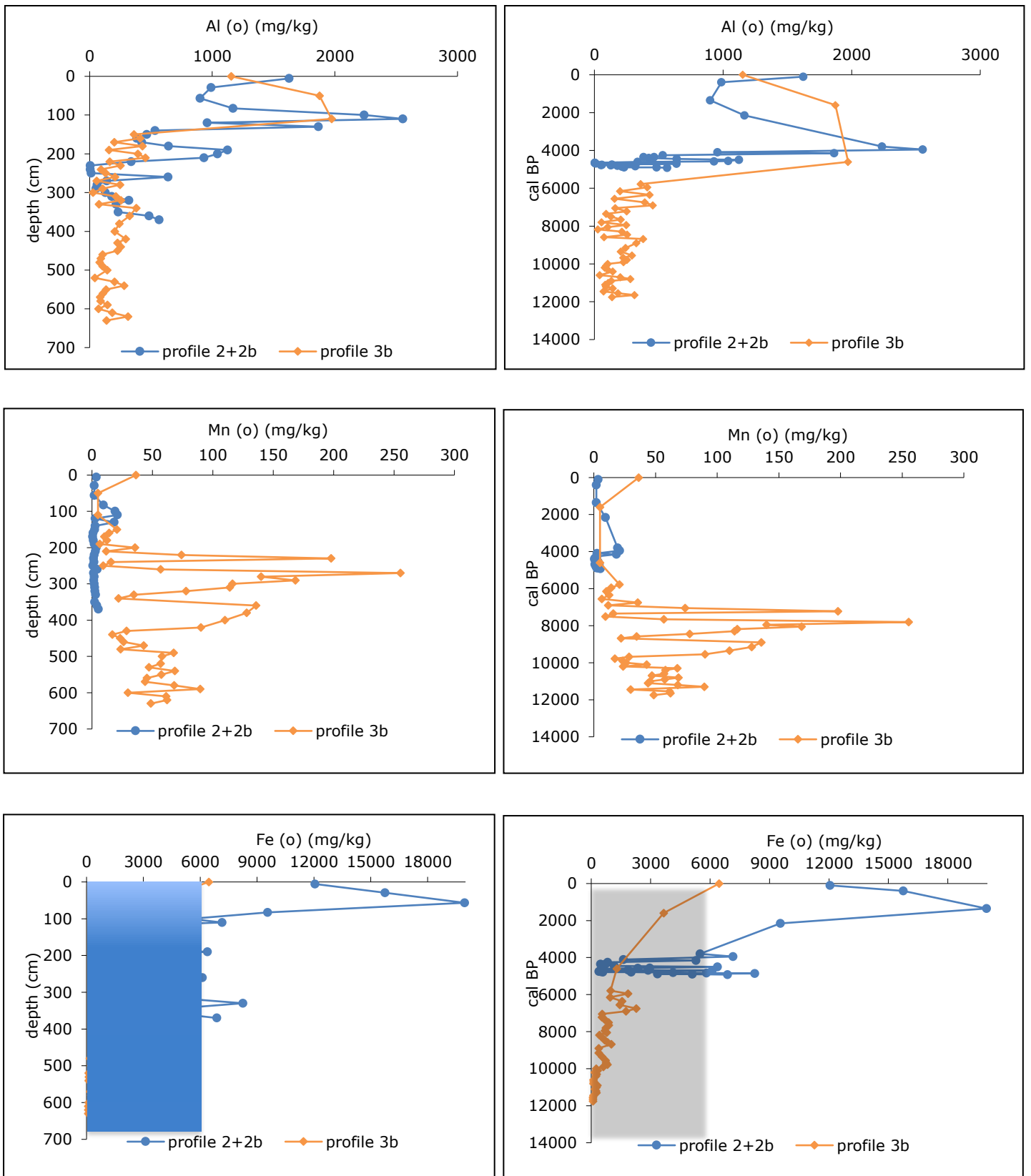


Figure 14: The six diagrams show the Mn, Fe and Al contents of the profiles 2+2b and 3b in mg/kg, measured with the AAS method. In blue the range of the soil profiles around for Fe. The range of the Mn and Al values are higher or rather, cover more than the entire area.

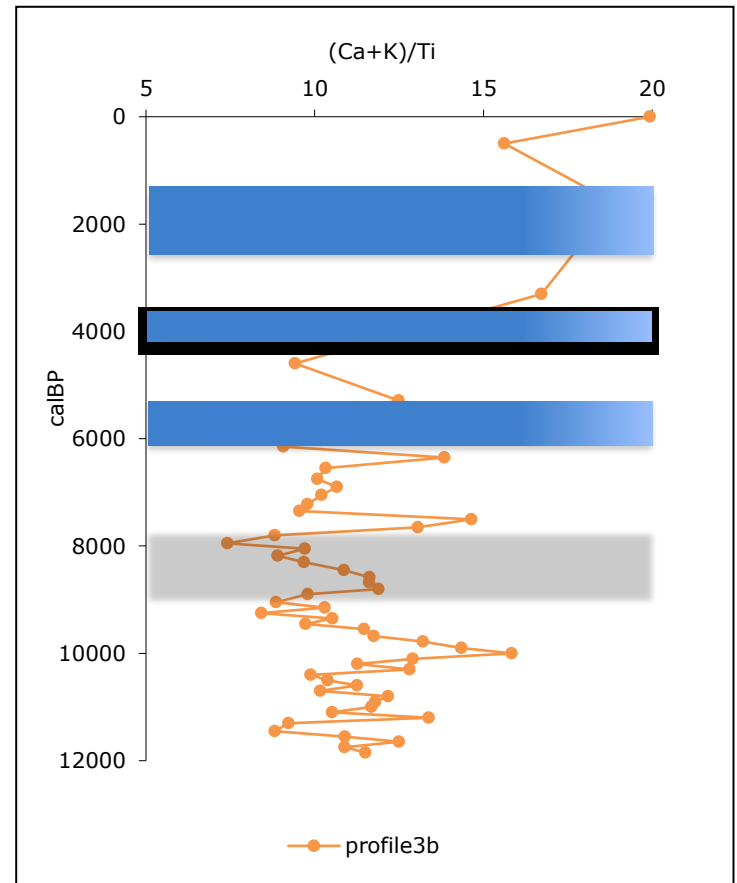
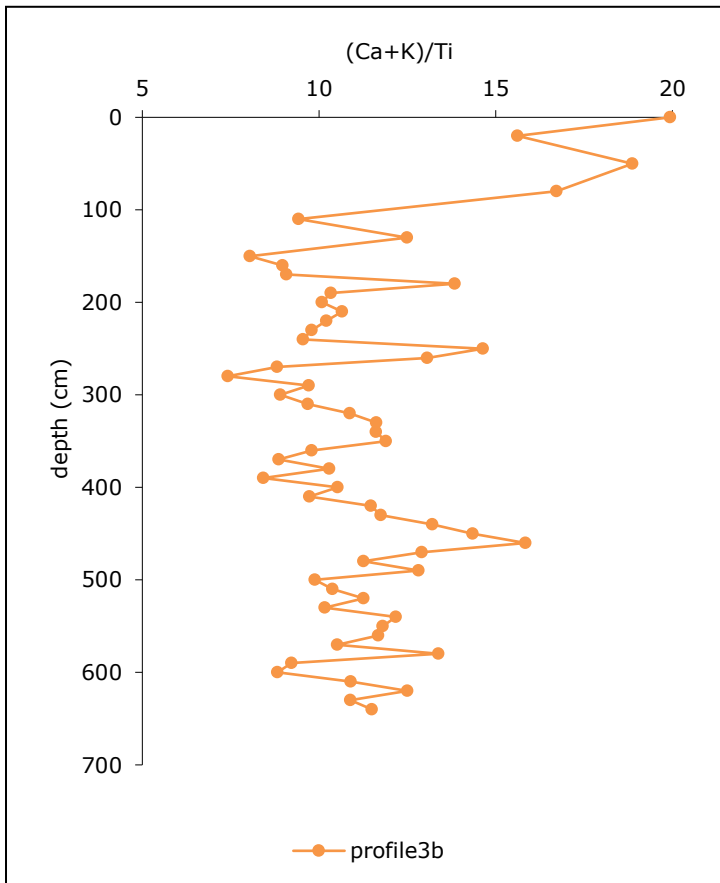
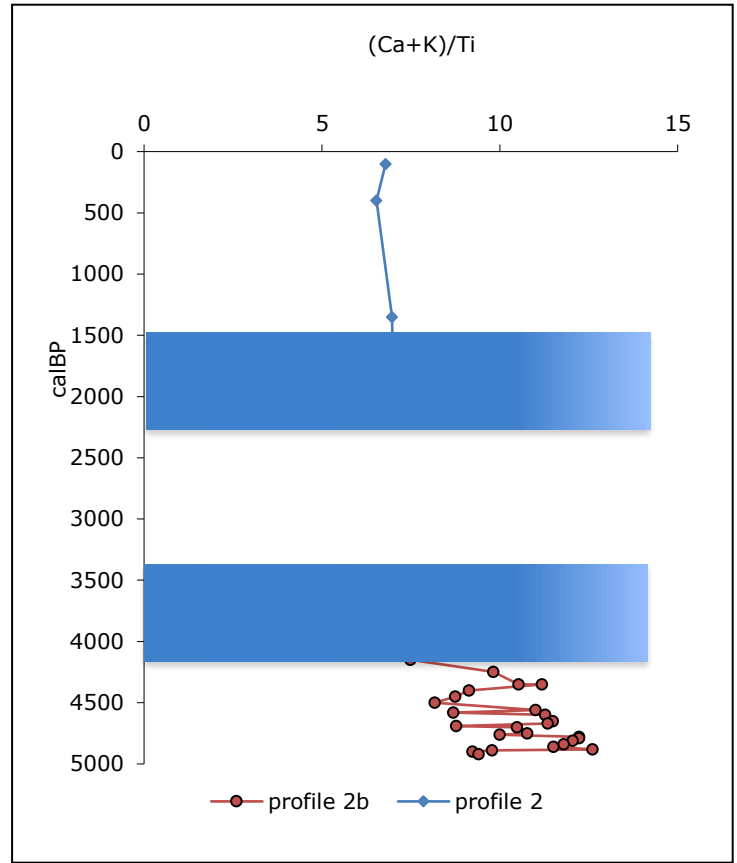
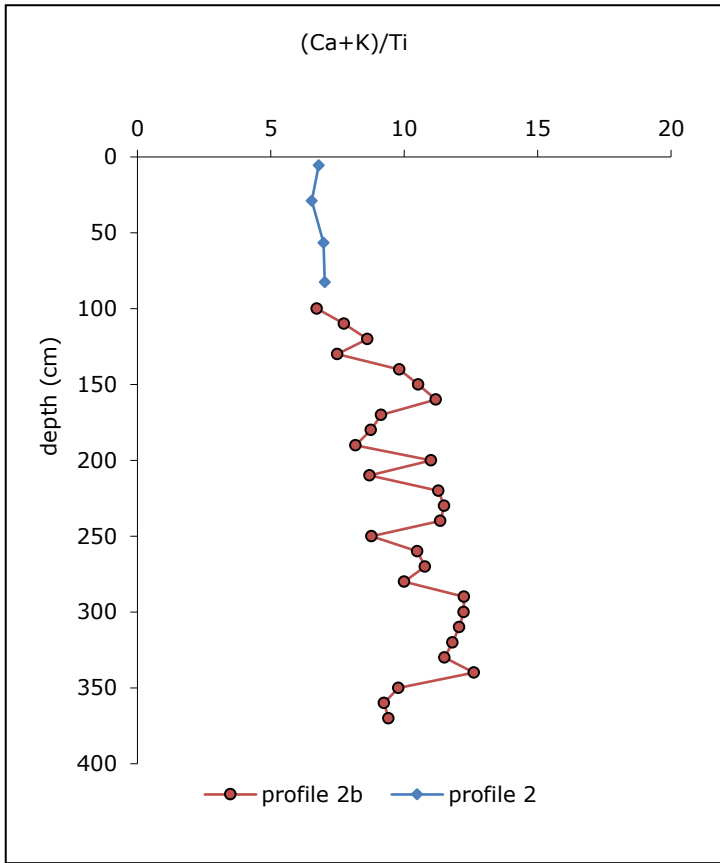


Figure 15: The four diagrams show the weathering index of profile 2+2b and 3b.

#### Ca+K / Ti

To estimate the weathering degree of the sediments, the molar ratios of (Ca+K)/Ti were used: the lower this ratio, the more advanced is weathering (Harrington and Whitney, 1987).

The (Ca+K)/Ti ratios of profile 3b exhibit a distinct change with increasing age towards lower values (Figure 15) We find the same trend along profile 2b. There, too, strong fluctuations >4000 calBP start. At ages < 4000 calBP the ratio remains in profile 2+2b and 1 rather stable between 5 and 10 . Profile 3 and 3b again show a locally different trend here. The ratio is around 15 until about 4000–6000 calBP. The (Ca+K)/Ti ratio is much lower at ages > 4000 calBP. Up to 4000 years, the ratio is mostly stable for all profiles except profile 1, where an unstable phase already occurs at 2500 years. It is interesting to note that the (Ca+K)/Ti value the range of profile 2 + 2b is quite different from the other profiles. The values remain mostly in a range of 5 – 10.

#### K/Rb

K/Rb and Ti/Zr ratios are commonly applied to determine changes in lithogenic sources (Silva-Sánchez et al., 2015). Rb is strongly linked to K, whereby the bond forms of Rb to silicates appear stronger than those with K (Kabara-Pendias, 2000). Therefore the K/Rb ratio may also indicate weathering processes because it becomes continuously smaller during soil formation processes.

Similar to the (Ca+K)/Ti ratio, an increasing variability can also be seen in profile 2+2b. In profile 3b this instability follows only from the year 6000. The fluctuations become larger. But a local trend can also be seen here. Profiles 3b and 3 have at 4000 calBP a value of 200, profiles 1 and 2+2b from 200 upwards.

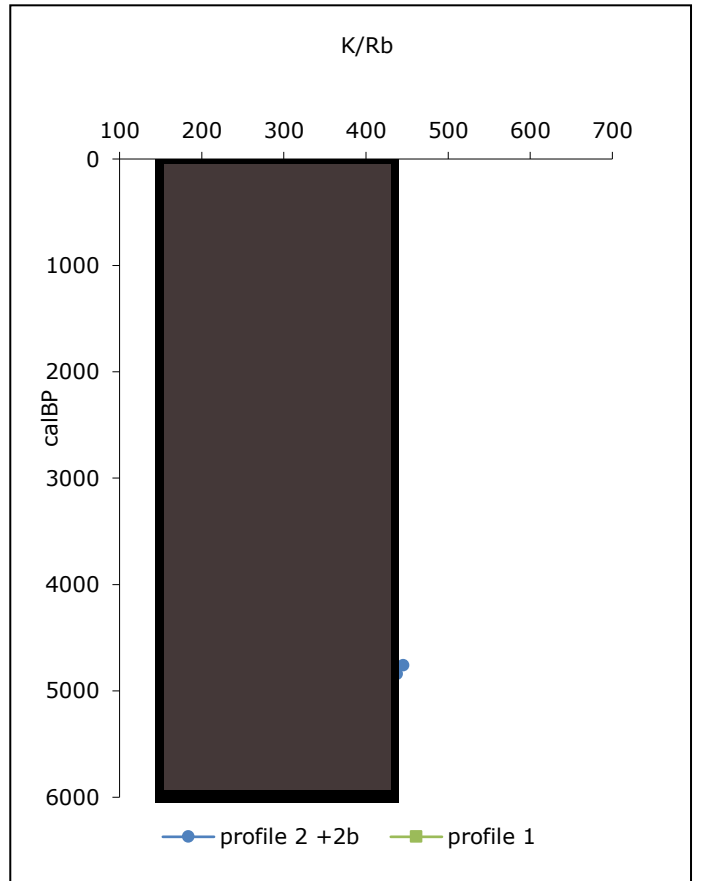
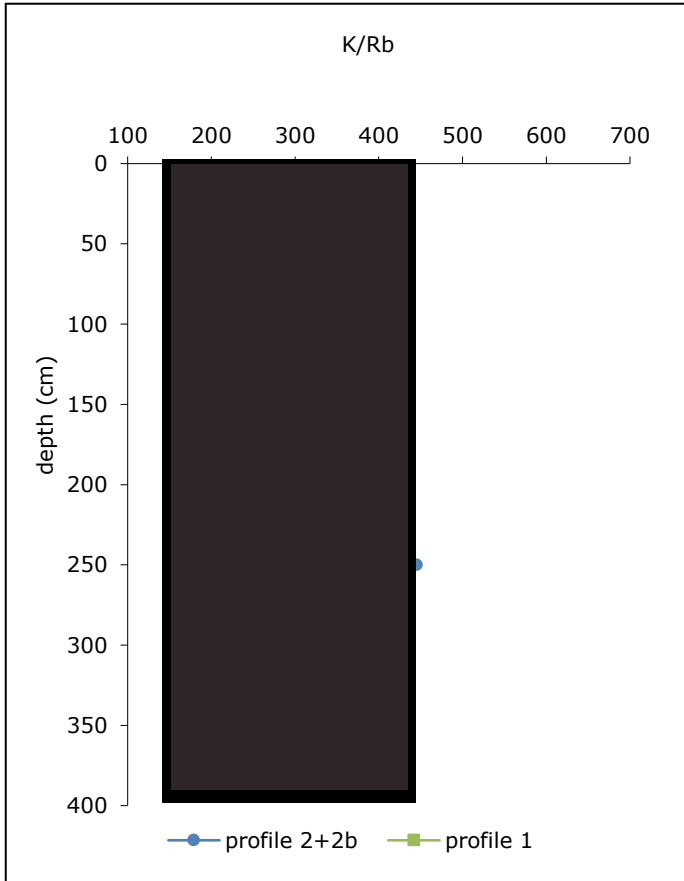
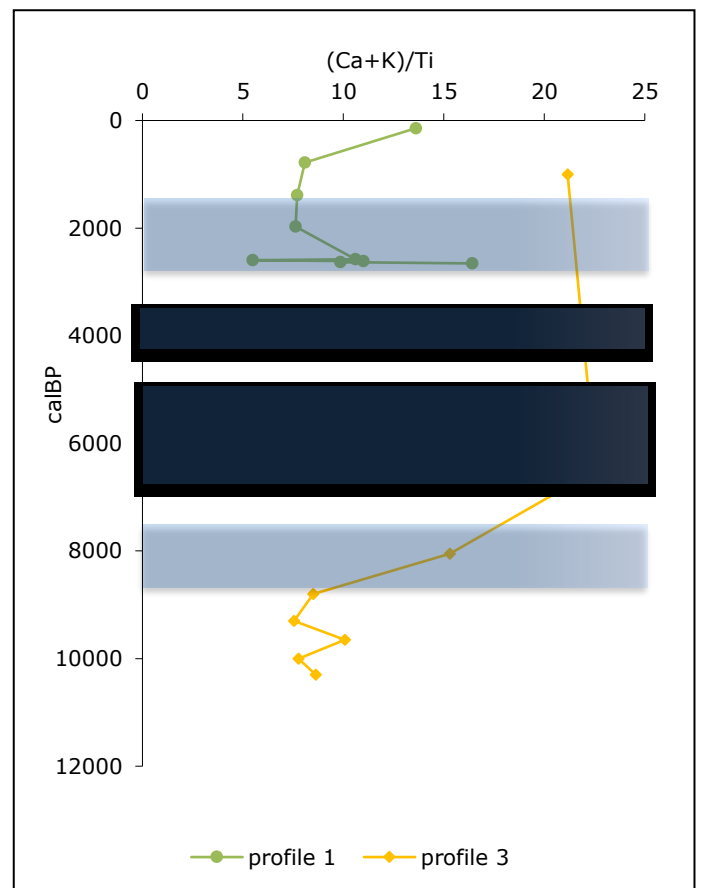
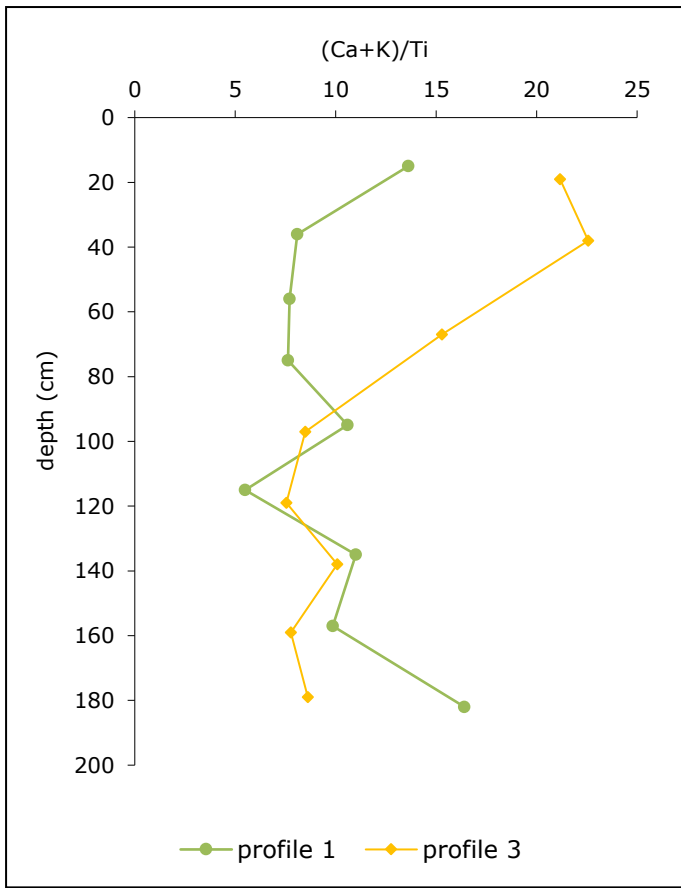


Figure 15: The two upper diagrams show the weathering index of profile 1 and 3. The two lower diagrams show the ratio of K and Rb and the range of soil profiles DP1-DP5 is shown in rose.

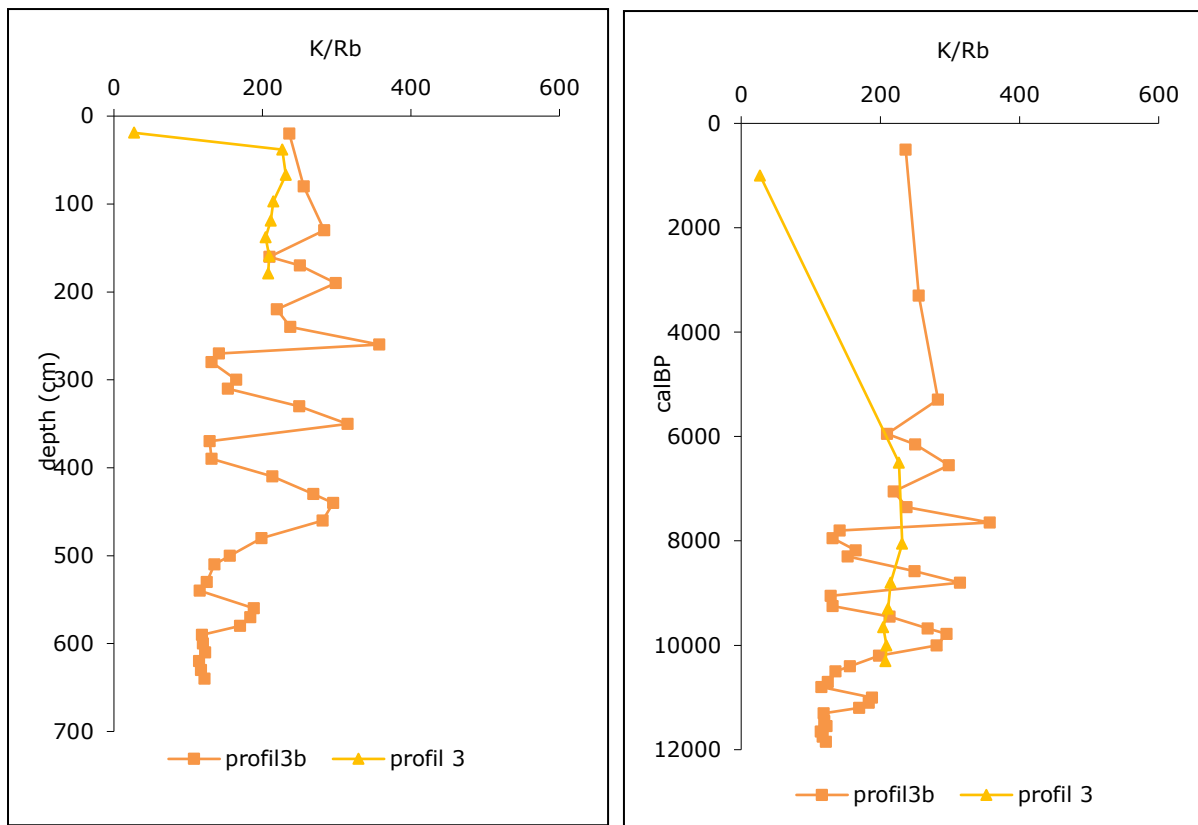


Figure 16: K/Rb ratio of the profiles 3 and 3b. in rose the range of the K/Rb ratio of the soil profiles DP1-DP5

#### Ti/Zr

The phenomenon of the high fluctuations around 4000 years, as previously seen with the two other indices, is also reflected in the Ti/Zr ratio. However, it can only be detected in profile 2+2b and 3b. With profile 3 the value increases continuously. But the values for profiles 3 and 3b are again within the same range, similar to profiles 1 and 2+2b.

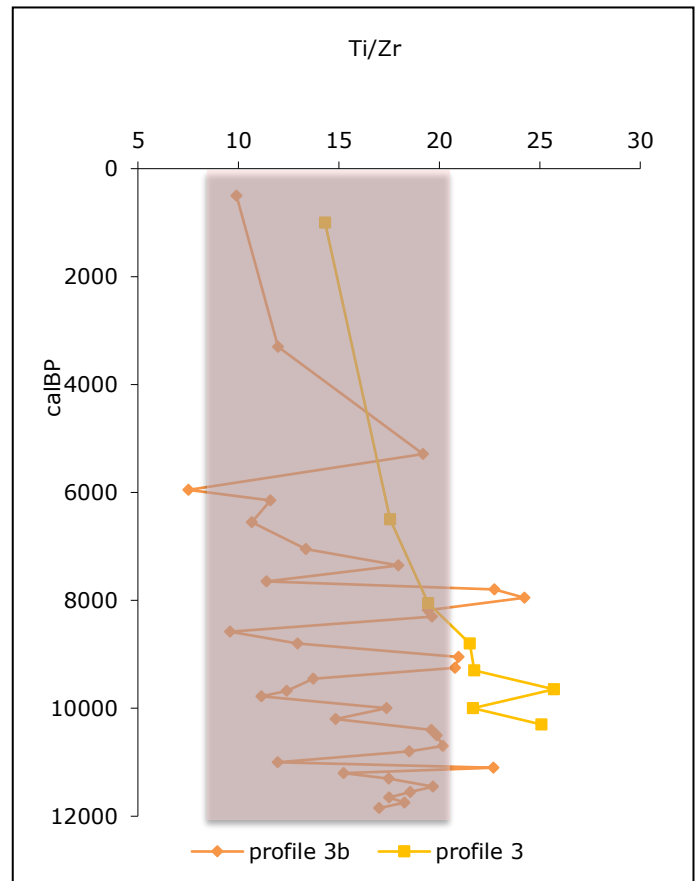
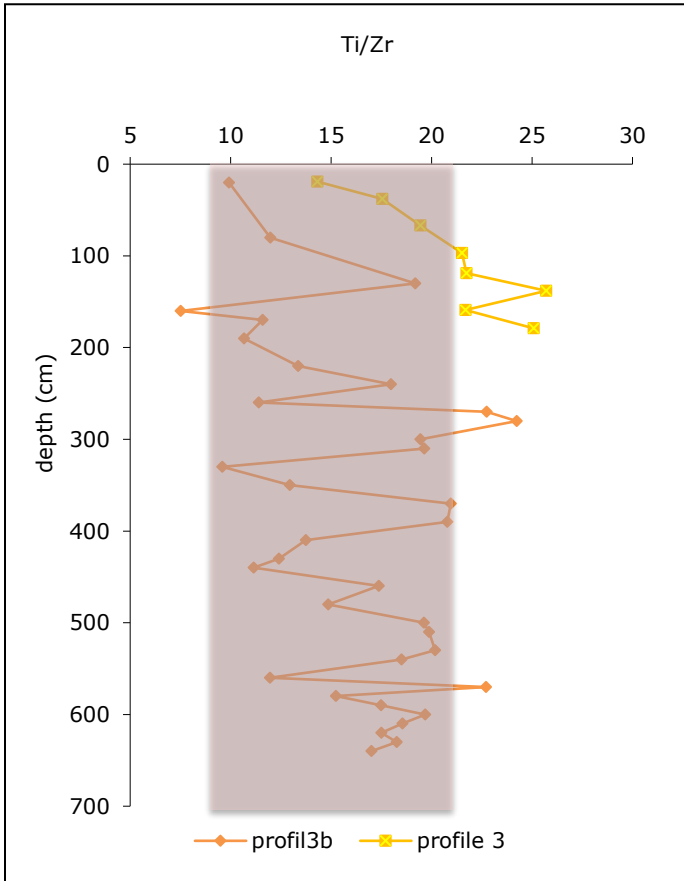
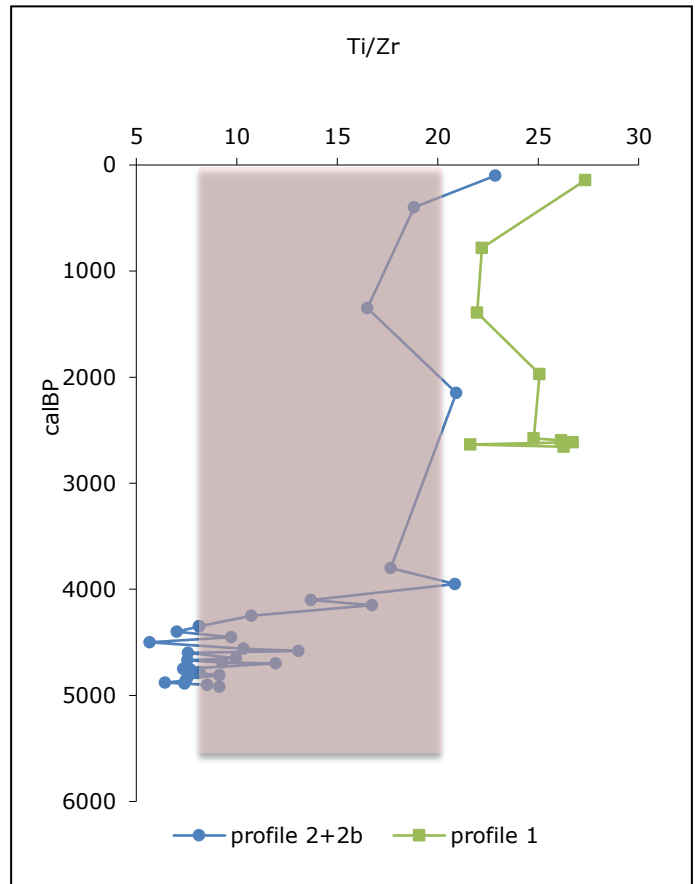
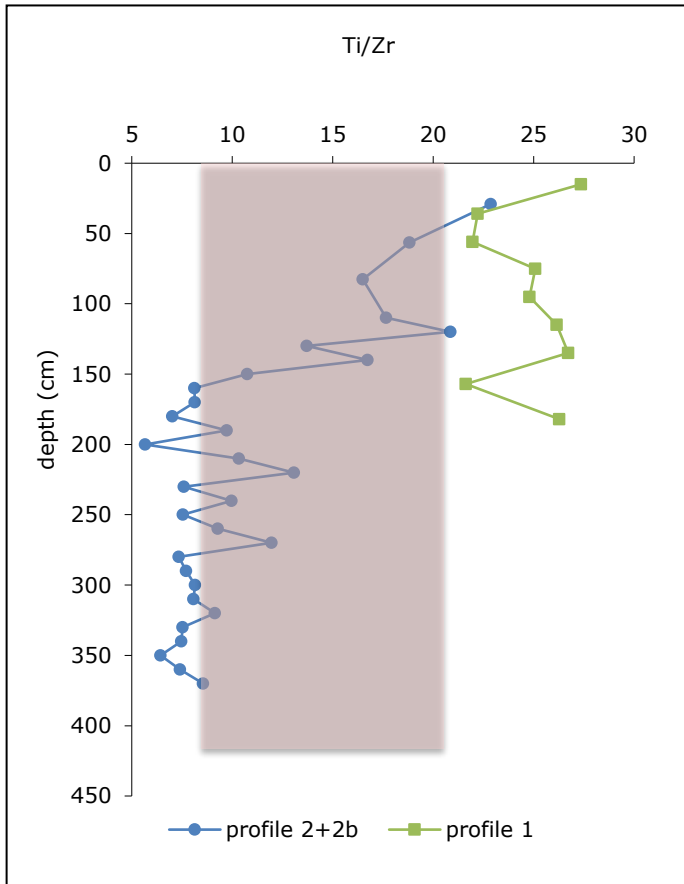


Figure 17: The four diagrams show the Ti/Zr ratio for the profiles 1,2+2b, 3 and 3b



## 4. Discussion

The overview of the C14 data shows that the expected age was not reached. We assumed that the ages were closer to the  $^{10}\text{Be}$  measurements of the rock boulders and should reach  $< 20$  ka. All C14 data are in the MIS 1, but if we have a look at the beryllium data, an age of up to 537 ka is reached. Obviously, the mire formed predominantly during the Holocene. We were able to drill down to about 640 cm but we unfortunately obtained 14-C ages, due to the lack of organic remains, only down to a depth of 420 cm. Thus the measured age dating between the  $^{10}\text{Be}$  measurement and the  $^{14}\text{C}$  measurements is very different. An unanswered question is also: how deep are the sediment deposits and the mire and where starts the bedrock.

The time gap between the deposition of inorganic and organic sedimentations cannot be clarified exactly. But it certainly took time (several hundreds of years) after the ice retreated and vegetation started to develop (Boxleitner, et al., 2017).

Our data show that the age-depth trends vary considerably between the investigated profiles.

The 14C data along the drilling cores have a different trend, which cannot always be explained exactly. If one first considers profiles 3 and 3b, which were taken very closely to each other, two different trends were obtained. In addition, there were several measurements that we had to exclude from the depth-age trend calculation due to plausibility reasons. Some data seemed unrealistic probably due difficulties during sampling. It seems likely that sometimes material from upper layers was moved to greater depth by using the vibration driller.

For the calculation of the sedimentation rate, an estimate had to be done using the corrected age-depth Profiles 3 and 3b are very similar and increasing slightly with age, while profiles 1 and profile 2+2b show a higher sedimentation rate from 2000 and 4000 calBP. There the increase is much stronger with increasing age, which is due to modeling the sedimentation rate.

However, the obtained sedimentation rates are only an approximation and should be considered with caution, especially with respect to the data for the lowest part of the sediment. There the curve was only interpolated.

It is difficult to explain why the age depth trend of profiles 3b and 3 is not the same, especially because these profiles are so close to each other. In addition, the question arises why no older material was found in all other measurements. A closer look at parameters other than age, we clearly see that they exhibit a quite similar depth trend in profiles 3 and 3b. It is precisely the increase of the sedimentation rate, both in profile 1 and profile 2+2b, that can be explained by the fact that the temperature rose again (Schönwieser, 1995), thus increasing the erosion rate. The increase in the sedimentation rate at profile 3b from 6000 calBP (until 10000 calBP), is characterized by a warm phase, which has existed over a longer period of time (almost 2000 years). It is interesting to see, however, that the sedimentation rate of profiles 3 and 3b never reach such high values when compared to the other two profiles. It is also interesting to note that profile 2+2b and profile 1 react so differently, respectively delayed with the

significant increase in sedimentation rate. A part of the strongly increasing sedimentation rate can be explained by the approximation of the age-deep trend curve. There is no clear trend to see if there has been an increase in the sedimentation rate during warm or cold phases. This is especially the case with an overview of all profiles. In individual profiles one can see the signals of the change of warm and cold phases in the sedimentation rate. Thus, the sedimentation rate usually increases after a cold phase: in profile 1, after the cold phase around 2000 years; in profile 2+2b after the cold phase around 4000 years; in profile 3b after the cold phase around 6000 years BP and in profile 3 after the cold phase around 8200 years BP. It is not really clear why signals of changing environmental conditions appear in some profiles and not in all. With respect to the sedimentation rate, however, it is noticeable that the sedimentation rate increases with the general warming in the Holocene, except profile 1, as warmer phases tend to generate larger sediment inputs (Boxleitner, et al., 2017).

The LOI values are very similar in the profiles 3 and 3b. Higher LOI values were measured in the upper horizons of profiles 3 and 3b than in the other profiles. In addition, the development of profiles 3 and 3b is very similar with increasing depth. At a depth around 150 cm, the LOI value decreases significantly in all profiles. There also the sample material changed a lot. The material became increasingly gravelly. And the question arises as to when the mire was created in its present form and state. If we take the different age trends

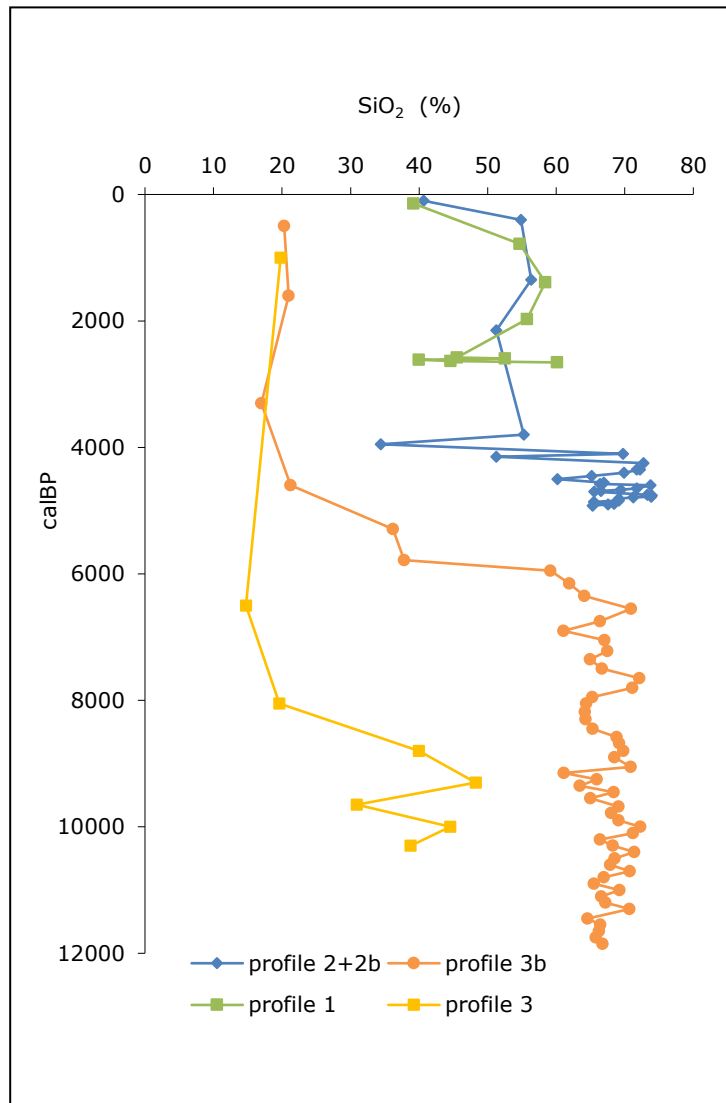


Figure 18: SiO<sub>2</sub> values for all profiles in %:

of the four drill cores and a depth of about 1.5 m, one could assume that the mire has developed from west to east. This would mean that the mire at the location of Profile 1 only developed about 2500 years ago and that at the location of Profile 2 +2b about 4000 years ago.

In the Holocene, the Earth was shaped by various phases in which the climate changed abruptly in a very short time (Booth, et al. 2005). In the middle of the 18<sup>th</sup> century there was the last little ice age, which is well documented by the advance of glaciers and their moraines, but also by tree year rings in

North America (Kenneth Lee, 1994). The climate must have been colder and at the same time drier, if one examines the tree rings of that time (Petersen, 1994). The change in vegetation also leads to the conclusion that a cooling occurred after 2650 calBP, with a shorter vegetation period (Whitlock, et al., 2011). Around 4.2 ka BP, in the Subboreal chronozone, the climate became again abruptly colder, followed by a rapid change of environment in North America (Booth, et al. 2005).

North America has experienced a significant cooling of the climate between 6000 and 5000 calBP, which has also resulted in increased precipitation during this cold period (Lauriol, et al., 2009). At 8.2 ka BP in the Boreal chronozone, there was a very strong climate change all over the world, triggered by a hitherto unknown and uncertain factor. Overall it became cooler and drier in the world. In the Rocky Mountains even more windy (Alley, et al., 1997; Berger et al., 2009). The weathering indices of the cores reveal a complex evolution of the mire. A certain lithological discontinuity within some profiles shows that erosion and accumulation processes were part of the mire's history. Profile 3 is a disturbance-free profile in terms of weathering. Around the year 6000, weathering conditions increased rapidly and stabilized again around the 9000 calBP in the Preboreal chronozone. Looking at profile 1, the first trend is very similar to profile 2+2b, as well to profile 3b but there must have been a disturbance around 2500 calBP, because again younger and unweathered material was deposited. This could be explained by strong erosional processes of the surrounding area (e.g. deposition of unweathered riverbed sediments). Nevertheless, it must be said that the explanation of soil dynamics over time is a very challenging task (Egli & Poulénard, 2017).

Looking at profile 3b, one can see the complexity of soil evolution. Again, the least weathered material is in the upper part indicating a strongly erosional phase in the surroundings.

From 4000 calBP, the weathering history of the profile becomes very complex. Strong fluctuations, over a short time period, in accumulation and erosion must have alternated. In profile 2 + 2b, and similar to profile 3b, there are very complex patterns of the weathering index from the 4000 calBP onwards. The lower horizons of the profile seem to be less weathered than the upper ones.

Looking at the Ti/Zr and K/Rb ratios, it is clear that most of the data are consistent with those from the soil profiles. With the profile 2+2b it is obvious that between 4000 and 5000 calBP the values do not fit into the range and are too low. These could partly be explained by the fact that material was introduced into the mire by aeolian entry. If one compares the values with those of Dahms and Egli (2016), who examined the area south-east to the mire on the terraces, one sees that there the range (6.4-17.4 for Ti/Zr) of the ratio is lower than that of the soil profiles around the mire. Also around 6000 calBP, the ratio of Ti/Zr decreases in the profile 3b and the sedimentation rate increases. Consequently aeolian material could have been deposited here as well. Looking at the K/Rb ratios, they fit very well into the range of soil profiles DP1-DP5. From about 4000 calBP the fluctuations of Ti/Zr in profile 2 + 2b are very strong. A similar process with many fluctuations takes place in profile 3b from about 6000 calBP. In profile 1, the ratio of Ti/Zr is outside the range of the soil profiles. These outliers cannot be explained.

If one considers the pH values of the mire cores, then they do not correspond to the original expectations. In the profile 3, the pH-value increases slightly at the beginning and then decreases slightly again. However, the (Ca+K)/Ti value changes much more. In profile 3 it is shown that the pH value and the (Ca+K)/Ti index behave similarly and indicate the same age trend. In the profiles 1, 3 and 3b, the weathering index (Ca+K)/Ti decreases with depth and thus with age. Only profiles 2+ 2b have a slight increase and less weathered material can be found at greater depth. The soil profiles east of the mire

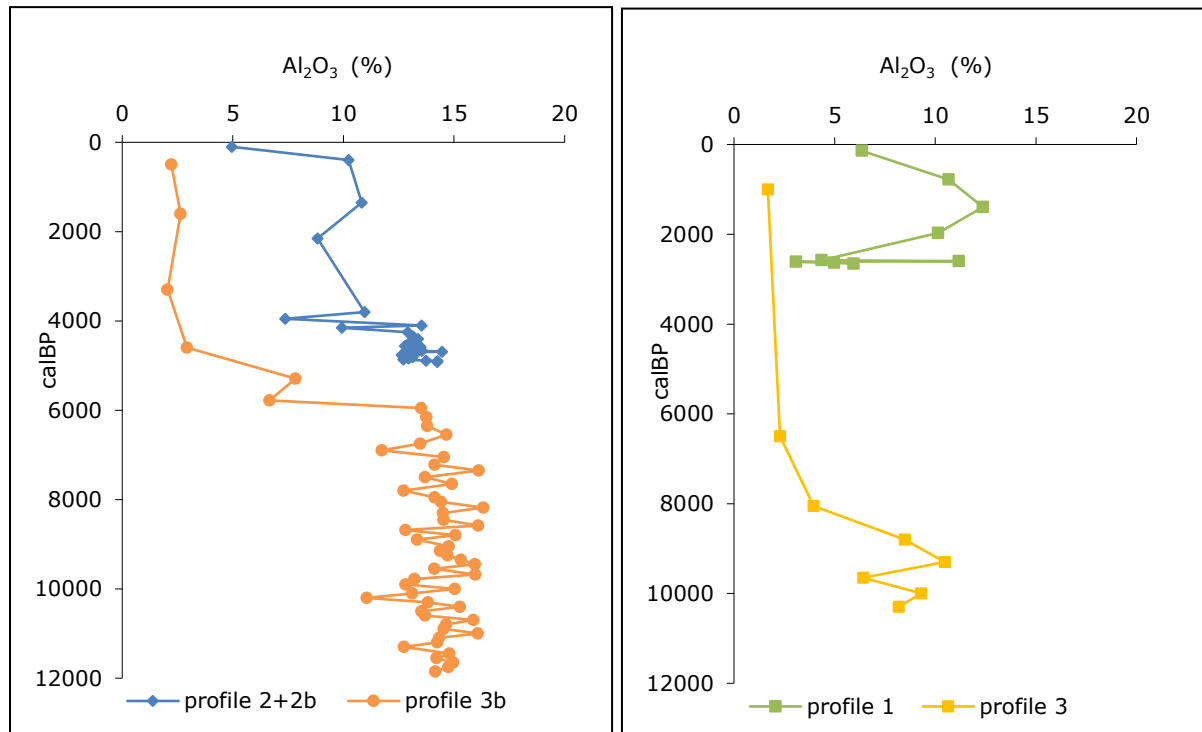


Figure 19: Al<sub>2</sub>O<sub>3</sub> concentrations (as an indicator of detritus input) along the profiles 2+2b, 3b and on the right diagram the profiles 1 and 3.

seem to be younger than DP1-DP3, because they have less weathered material according to the (Ca+K)/Ti value. If one considers different indicators such as the (Ca+K)/Ti ratio, the Si contents or the LOI values in the upper horizons of the cores, one sees a clear locality trend. This means that profiles 3b and 3 have similar values but are clearly different from the profiles 2+2b and 1. Such correlations can also be seen in the pH value. The question arises whether the different regions of the mire have received different material input or whether, as already assumed above, they have developed individually at different times.

Looking at the concentration of Al<sub>2</sub>O<sub>3</sub> there is no clear trend of warm or cold periods in which there were higher detritus inputs. After about 6000 calBP the concentration increases strongly. A similar, but less pronounced trend can be seen in profile 3. This means that 6000 years ago the detritus input decreased rapidly. What can be clearly seen with the Al<sub>2</sub>O<sub>3</sub> value is that with age the content of Al<sub>2</sub>O<sub>3</sub>

generally increases. Only in profile 1, around 2000 calBP a decrease was detected, which cannot be explained. The exact same trend can also be seen in the SiO<sub>2</sub> content.

Noteworthy is also that the values of profile 3b rise significantly around 6000 calBP and then remain at a high level with increasing age.

In general, the organic carbon content and LOI decrease with increasing profile depth in the mire. This can be attributed to the fact that the input material is mainly granite (Dahms & Egli, 2016) and that at colder periods there was hardly any organic material input.

Having a closer look at the Al (o) values of the soils and the profiles, we can notice that they are in a similar range. Only soil profile DP5 with it is almost 5000 mg/kg on the surface is outside the range.

This soil profile is also the farthest away from the mire cores.

Another point that has not yet been clarified is why is the Fe value in the drill cores are much higher than in the soil profiles. In the soil profiles, Fe-contents of about 6000 mg/kg are reached whereas in the mire cores values up to 18000 mg/kg were measured. Higher Fe(o) values in the mires are probably due to the reducing conditions (low redox potential) and therefore a higher mobility of Fe and detachment from primary minerals.

The DRIFT analyses gave no additional insight for a deeper understanding of the previously mentioned processes. DRIFT however reveals, that kaolinite is present in all samples. Kaolinite may derive from aeolian deposits (Boxleitner et al., 2017) or the weathering of plagioclase or phyllosilicates. Gibbsite as a product of weathered silicates is found in soil profiles, especially DP3, but also in the drill cores. The

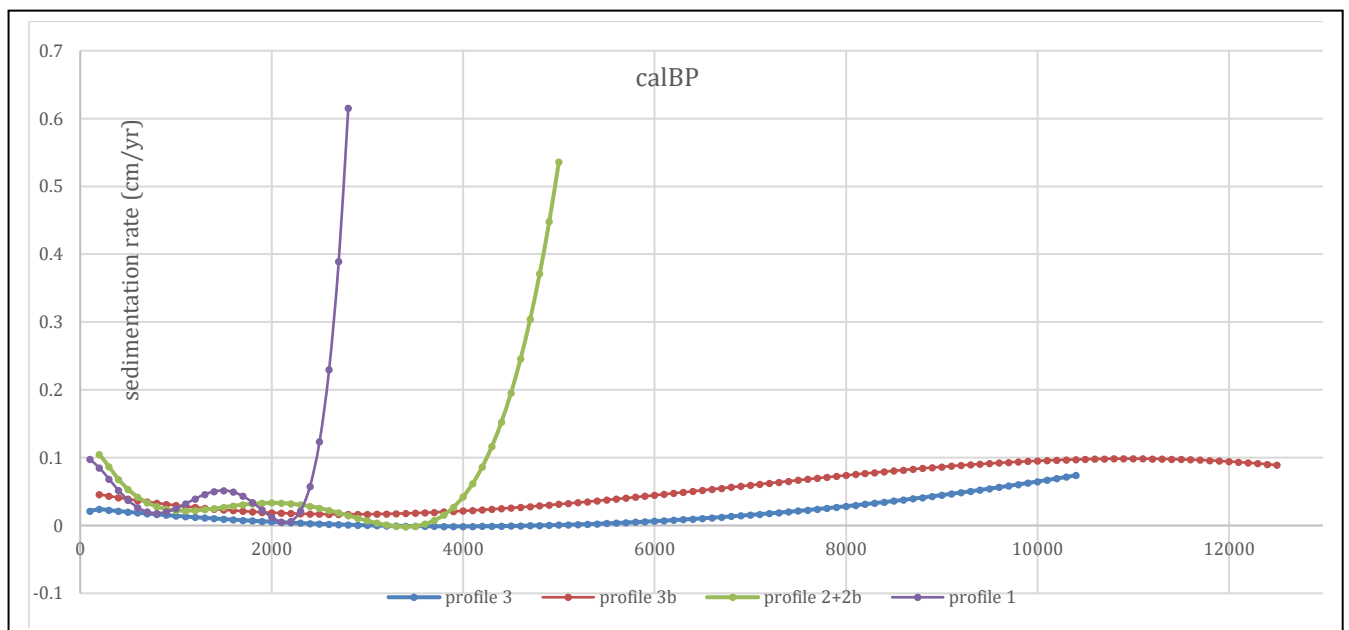


Figure 20: The calculated sedimentation rates of soil profiles 1, 2+2b,3 and 3b and in the upper figure the SiO<sub>2</sub> content in % for all mire profiles.

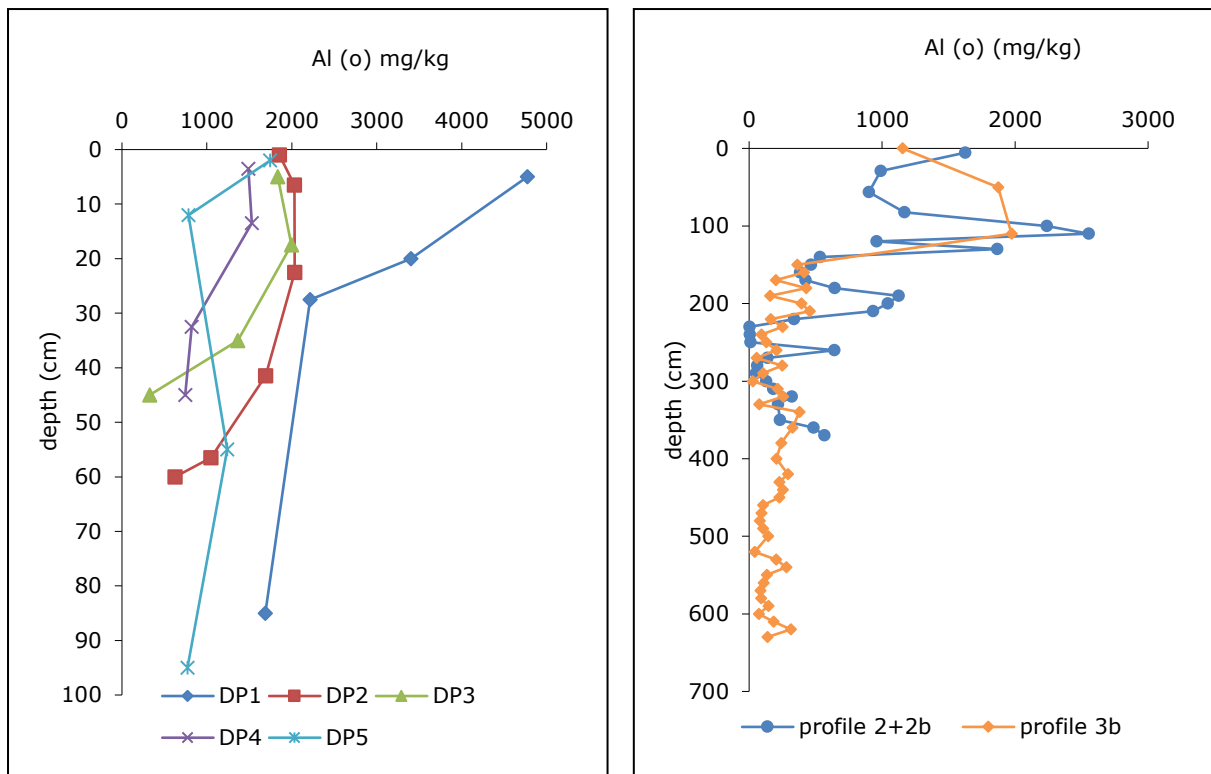


Figure 21: Al (o) Values of the soil profiles and the drill cores from the mires for comparison.

DRIFT analysis reflects the granitic characteristics of the deposits due to the presence of mica and quartz at all depths. Almost everywhere kaolinite could be found in the soil profiles, confirmed by the XRD and DRIFT analyses.

In one wide step and for further investigation I will make some changes. First of all, it would be very interesting to know how deep the mire are and where the original rock begins. For this purpose, I would choose a different drill. The VibraCore is not suitable for such a terrain but also material. The handling is cumbersome and due to the vibration the damp and unstable mire soil is easily moved and transported to the wrong places. I would also drill further in the west and east of the mire. Because the differences between the profiles were already very large. It would be exciting to know whether these differences are increasing and whether the mire has really developed differently at the various locations. Coming back to the hypothesis and the research questions we must note that the moor is not older than 50000 years, but much younger, at least in the depths we could investigate. It can also be said that the sedimentation rate changes over time. However, this change is very different depending on the profile and no general trend can be observed.

## 5. Conclusion

It is very difficult to see a very clear trend in soil developments in many respects, because they are often non-linear processes and chronosequences can be disturbed by other factors (Dahms et al., 2012). Also in Dickinson Park there were big differences between the individual profiles. Nevertheless, some things can be noticed.

1. The maximum age of the soil in the mire is 10245-10188 calBP and so there is a big difference between the moraine deposits and the development of the mire.
2. There is a locality trend of the profiles in relation to different values, such as the pH or LOI values.
3. There must have been some aeolian entry into the mire.
4. The mire has reacted differently to past climate changes and this reaction is very different from profile to profile.
5. Not all profiles have the same age.

Geochemical tracers in combination with C14 analyses allow a reconstitution of a mire formation and can decipher the landscape processes (Boxleitner, et al. 2017).

The geochemical tracers show that the moor formation has been altered by the climate. After the cold phases, the sedimentation phase usually increased. The cooling phases are around 2650, 5000 and 6000 and 8200 calBP. It can be seen that not all profiles react equally to these climate fluctuations. Some seem to be more stable and less strongly influenced by them, with a larger time delay. In addition, it can be seen that both the granitic bedrock from the surrounding area and the aeolian input contribute to the sedimentation input. There are phases with increased sediment input. If one looks at the values of pH or LOI, one can see that these are very different between the individual profiles. However, you can also see that there is a certain locality trend. Profiles 3 and 3b behave similarly in their values. The same can be seen with profiles 2+2b and 1. This may lead to the conclusion that the moor has developed in different places at different times in different ways. The different ages of the individual profiles also indicate a different development. Due to the age, we can say that there was a long-time delay between the moraine deposits and the development of the mire. The mire itself is not as old as expected with its 102045-10188 calBP. Also the sediment rate is very different between the profiles, but there is also a locality trend. Thus the profiles in the east of the mire reach higher values than the profiles 3 and 3b. Further research and field work is certainly needed to find out more about the development of the mire in Dickinson Park and to get a more accurate idea of how the mire reacted to the environment. Nevertheless, mires remain an important archive for the reconstruction of the past climate conditions.

## 6. Acknowledgments

I would like to thank Dr. Prof. Markus Egli for his great support of my master thesis, his professional and very good feedback during the whole process. I would also like to thank Dennis Dahms and Taylor Garton for their help in the field work and that I was able to participate in this project. I would also like to thank Tatjana Kraut and Tomy Keller for their support during the laboratory time. I would also like to thank the GEGZ for the financial support for my field work.



## 7. References

- AABY, B. 1976. Cyclic climatic variations in climate over the past 5500 years reflected in raised bogs. *Nature*, 263, 281-284.
- ALFELD, M., Requena, G., Boesenberg, U., Bauckhage, C., Wellenreuther, G., Falkenberg, G., Whabza, M. 2016. Non-negative matrix factorization for the near real-time interpretation of absorption effect in elemental distribution images acquired by X-ray fluorescence imaging. *Journal of Synchrotron Radiation*, Vol 23, 579-589.
- ALLEY, R.B., Mayewski, P.A., Sowers, T., Stuiver, M., Tayler, K.C. and Clark, P.U. 1997. Holocene climatic instability: A prominent, widespread event 8200 yr. ago, *Geology* 25;483-486.
- APARICIO, P., Ray, E., Ferrell, Galán, E. 2010 Mg and K exchange cation effects on the XRD analysis of soil clays, *Philosophical Magazine*, 90:17-18, 2373-2385, DOI: 10.1080/14786430903559417.
- BLAAUW, M. 2010. Methods and code for 'classical' age-modelling of radiocarbon sequences. *Quaternary Geochronology* 5, 512-518.
- BERGER, J.F., Guilaine, J. 2009. The 8200 calBP abrupt environmental change and the Neolithic transition: a Mediterranean perspective. *Quat. Int.* 200, 31–49.
- BOOTH, R.K., Jackson, S.T., Forman, S.L., Kutzbach, J.E., Bettis, I. E.A., Kreig, J., Wright, D.K. 2005. A severe centennial-scale drought in midcontinental North America 4200 years ago and apparent global linkages. *The Holocene* 15, 321–328.
- BOXLEITNER, M., Musso, A., Waroszewski, J., Makiewicz, M., Maisch, M., Dahms, D., Brandová, D., Christl, M., de Castro Portes, R., Egli, M. 2017. Late Pleistocene – Holocene surface processes and landscape evolution in the central Swiss Alps. *Geomorphology* 295, 306-322.
- BRONK-RAMSEY, C. 2001. Development of the radiocarbon calibration program. *Radiocarbon* 43, 355–363.
- BRONK-RAMSEY, C., 2009. Bayesian analysis of radiocarbon dates. *Radiocarbon* 51, 337–360.
- BRONK-RAMSEY, C., Dee, M., Lee, S., Nakagawa, T., Staff, R. 2010. Developments in the calibration and modelling of radiocarbon dates. *Radiocarbon*, 52, 953-961.
- BURGA CA. (1979): Postglaziale Klimaschwankungen in Pollendiagrammen der Schweiz. *Vierteljahresschrift Naturforschende Gesellschaft Zürich*, 124, 265-283.
- CHAMBERS, F.M., Booth, R.K., De Vleeschouwer, F., Lamentowicz, M., Le Roux, G., Mauquoy, D., Nichols, J.E., van Geel, B., 2012. Development and refinement of proxy-climate indicators from peats. *Quaternary International* 268, 21–33.
- COPELAND, H.E., S.A. Tessman, S.A., Girvetz, E.H., Roberts, L., Enquist, C., Orabona, A., Patla, S., Kiesecker, J. 2010. A geospatial assessment on the distribution, condition, and vulnerability of Wyoming's wetlands. *Ecological Indicators* 10: 869-879.

- DAHMS, D., Favilli, F., Krebs, R., Egli, M. 2012. Soil weathering and accumulation rates of oxalate-extractable phases derived from alpine chronosequences of up to 1Ma in age. *Geomorphology*, 151,99-113.
- DAHMS, D., Egli, M. 2016. Carbonate and elemental accumulation rates in arid soils of mi-to-late Pleistocene outwash terraces, southeastern Wind River Range, Wyoming, USA. *Chemical Geology* 446, 147-162.
- DIXON, J.B., Weed, S.B. 1989. *Mineralien in Bodenumgebungen*, 2. Madison, WI: Soil Science Society of America.
- EGLI, M., Poulencard, J., 2017. Soils of mountains landscapes. *The International Encyclopedia of Geography*. 1-6.
- EGLI, M., Lessovaia, S.N., Chistayakov, K., Inozemzev, S., Polekhovsky, Y., Ganyushkin, D. 2015. Microclimate affects soil chemical and mineralogical properties of cold alpine soils of the Altai Mountains (Russia). *Journal of Soils and Sediments* 15, 1420-1436.
- EGLI, M., Kraut, T., Brandova, D., Keller, T. and De Castro Portes, R. 2018. *Geochronology laboratory methods*, University of Zurich, Department of Geography.
- EGLI, M., Merkli, C., Sartori, G., Mirabella, A., Plötze, M. 2008. Weathering, mineralogical evolution and soil organic matter along a Holocene soil toposequence on carbonate-rich materials. *Geomorphology*, 97, 675-696.
- ESSL, F., Dullinger, S., Moser, D., Rabitsch, W. Kleinbauer, I., 2011. Vulnerability of mires under climate change: implications for nature conservation and climate change adaptation. *Biodivers Conserv*, 21, 655-669.
- GARCÍA, R., Báez, A.P. 2012. Atomic Absorption Spectrometry (AAS), *Atomic Absorption Spectroscopy*, 1-14.
- HARNOIS, L. 1988. The CIW index: a chemical index of weathering. *Sediment Geology* 55, 319–322.
- HARRINGTON, C.D., Whitney, J.W. 1987. Scanning electron microscope method of rock-varnish dating. *Geology* 15, 967–970.
- HEIDEL, B., 2013. Sensitive plant survey in the Dickinson Park area. Prepared for the Shoshone National Forest. Wyoming Natural Diversity Database, Laramie, WY.
- HILLIER, S. 2003. Quantitative analysis of clay and other minerals in sandstones by X-ray powder diffraction (XRPD). *Int. Assoc. Sedimentol. Spec. Publ.* 34, 213–251.
- HILTMANN, W. and Stribny, B. 1998. *Tonmineralogie und Bodenphysik – Handbuch zur Erkundung des Untergrundes von Deponien und Altlasten*, Band 5. Springer Verlag, Berlin/ Heidelberg.
- KABARA-PENDIAS, A., Pendias, H. 2000. *Trace elements in soils and plants*, Third Edition.
- KENNETH LEE, P., 1994. A Warm and Wet little Climatic optimum and a cold and dra little Ice Age in the southern Rocky Mountains, U.S.A.. *Climatic Change*. Vol 26, 243-269.

- MAVRIS, C., Furrer, G., Dahms, D., Anderson, S., Blum, A., Goetze, J., Wells, A., Egli, M. 2015. Decoding potential effects of climate and vegetation change on mineral weathering in alpine soils: an experimental study in the Wind River Range (Wyoming, USA). *Geoderma* 255-256, 12–26.
- MINASNY, B., McBratney, A.B., Brough, D.M., Jacquier, D. 2011. Models relating soil pH measurements in water and calcium chloride that incorporate electrolyte concentration. *European Journal of Soil Science*, 62, 728-732.
- MOORE, D.M. & Reynolds, R.C. 1997. X-ray diffraction and the identification and analysis of clay mineral. 2<sup>nd</sup> edition, Oxford University Press, New York.
- LANGDON, P., Hughs, P. and Brown, T. 2012. Peat stratigraphy and climate change. *Quaternary International* 268, 1-8.
- LANSON, B., 1997. Decomposition of experimental X-ray diffraction patterns (profile fitting): a convenient way to study clay minerals. *Clays and Clay Minerals* 45, 132-146.
- LAMENTOWITCZ, M., Galka, M., Lamentowicz, L., Obremnska, M., Köhl, N., Lücke, A., Jassey, V.E.J. 2015. Reconstructing climate change and ombrotrophic bog development during the last 4000 years in northern Poland using biotic proxies, stable isotopes and trait-based approach. *Palaeogeography, Palaeoclimatology, Palaeoecology*, Vol 418, 261-277
- LAURIO, B., Lacelle, D., Labrecque, S., Duguay, C.R., and Telka, A. 2009. Holocene Evolution of Lakes in the Bluefish Basin, Northern Yukon, Canada. *Arctic*, Vol 62, No 2, 212-224.
- LEMENTOWITZ, M., Slowinski, M., Marcisz, K., Zielinska, M., Kaliszan, K., Lapshina, E., Gilbert, D., Buttler, A., Fialkiewicz-Koziel, B., Jassey, V.E.J., Laggoun-Defarge, F., Kolaczek, P. 2015. Hydrological dynamics and fire history of the last 1300 years in western Siberia reconstructed from a high-resolution, ombrotrophic peat archive. *Quaternary Research*, Vol 84, 312-325.
- LEONARD, E., Plummer, M., Carrara, P. 2014. Numerical modeling of the Snowmass Creek paleoglacier, Colorado, and climate in the Rocky Mountains during the Bull Lake glaciation (MIS 5). *Quaternary Research* 82, 533-541.
- MOORE, D.M., Reynolds, R.C. 1997. X-ray diffraction and the identification and analysis of clay minerals. 2<sup>nd</sup> edition, Oxford University Press, New York.
- REIMER, P.J., Bard, E., Bayliss, A., Beck, J.W., Blackwell, P.G., Bronk-Ramsey, C., Buck, C.E., Cheng, H., Edwards, R.L., Friedrich, M., Grootes, P.M., Guilderson, T.P., Hafliðason, H., Hajdas, I., Hatté, C., Heaton, T.J., Hoffmann, D.L., Hogg, A.G., Hughen, K.A., Kaiser, K.F., Kromer, B., Manning, S.W., Nui, M., Reimer, R.W., Richards, D.A., Scott, E.M., Southon, J.R., Staff, A.R.A., Turney, C., van der Plicht, J. 2013. IntCal13 and Marine13 radiocarbon age calibration curves 0–50,000 years calBP. *Radiocarbon* 55, 1869-1887.
- ROWELL, D.L. 1994. *Bodenkunde: Untersuchungsmethoden und ihre Anwendungen*. Springer Verlag, Berlin/ Heidelberg.

- SATHIS KUMAR, Y.S., Naidu, M.V.S. 2011. Clay mineralogy of soils developed from granite-gneiss and alluvium in the Vadamalapeta mandai of Chittoor district, Andhra Pradesh, *Agropedology* 201, 52-55.
- SILVA-SÁNCHEZ, N., Schofield, J.E., Mighall, T.M., Cortizas, A.M., Edwards, K.J., Foster, I. 2015. Climate changes, lead pollution and soil erosion in south Greenland over the past 700 years. *Quat. Res.* 84, 159–173.
- SMITH, J. 2003. Aspects of the loss-on-ignition (loi) technique in the context of clay-rich, glaciolacustrine sediments, *Geografiska Annaler: Series A, Physical Geography* 85, 91-97.
- WALTHERT, L., Zimmermann, S., Blaser, P., Luster, J., Lüscher, P. 2004. *Waldböden der Schweiz. Band 1. Grundlagen für Region Jura.* Birmensdorf, Eidgenössische Forschungsanstalt WSL. Hep Verlag, Bern.
- WHITLOCK, C., Briles, C.E., Fernandes, C.M., Gage, J. 2011. Holocene vegetation, fire and climate history of the Sawtooth Range, central Idaho, USA. *Auanternary Researche* 75, 114-124.
- YOO, K., R. Amundson, A. M. Heimsath, W. E. Dietrich, and G. H. Brimhall (2007), Integration of geochemical massbalance with sediment transport to calculate rates of soil chemical weathering and transport on hillslopes, *J. Geophys. Res.*, 112, 1-15
- YU, Z., Eicher, U. 2019. Abrupt Climate Oscillations During the Last Deglaciation in Central America. *Science* 282, 2235-2238.
- ZIMMERMANN, M., Leifeld, J., Schmidt, M., Fuhrer, J. 2011. Characterization of Soil Properties by DRIFT-Spectroscopy. *Agroscope FAL Reckenholz, Swiss Federal Research for Agroecology and Agriculture and Geography Department of the University of Zurich.*
- ZOLLER, H., Schindler, C., Röthlisberger, H., 1966. Postglaziale Gletscherstände und Klimaschwankungen im Gotthardmassiv und Vorderrheingebiet. *Verhandlungen der Naturforschenden Gesellschaft Basel* 77, 97-164.
- ALFRED MATTHIAS, 2011, Schematischer Aufbau eines Röntgenfluoreszenzspektrometers, *Welt der Physik*. 6.6.2019  
<https://www.weltderphysik.de/gebiet/teilchen/licht/synchrotronstrahlung/roentgenfluoreszenzanalyse/roentgenfluoreszenzanalyse/>

# Master's thesis statement of originality

«Personal declaration: I hereby declare that the submitted thesis is the result of my own, independent work. All external sources are explicitly acknowledged in the thesis.»

31.08.2019

.....  
Place and Date

.....  
Signature

A handwritten signature in black ink, appearing to be 'A. Jantzen', is written over a light blue rectangular background. The signature is positioned above a horizontal dotted line.